Journal of Geophysical Research: Atmospheres

RESEARCH ARTICLE
10.1029/2018JD028768

Modeling of Atmospheric Aerosol Properties in the São Paulo Metropolitan Area: Impact of Biomass Burning

Angel Vara-Vela[1], Maria de Fátima Andrade[1], Yang Zhang[2], Prashant Kumar[3,4], Rita Yuri Ynoue[1], Carlos Eduardo Souto-Oliveira[5], Fábio Juliano da Silva Lopes[1,6], and Eduardo Landulfo[6]

[1]Department of Atmospheric Sciences, Institute of Astronomy, Geophysics and Atmospheric Sciences, University of São Paulo, São Paulo, Brazil, [2]Department of Marine, Earth and Atmospheric Sciences, College of Sciences, North Carolina State University, Raleigh, NC, USA, [3]Global Centre for Clean Air Research, Department of Civil and Environmental Engineering, Faculty of Engineering and Physical Sciences, University of Surrey, Guildford, UK, [4]Environmental Flow Research Centre, Faculty of Engineering and Physical Sciences, University of Surrey, Guildford, UK, [5]Geocronological Research Centre, Institute of Geosciences, University of São Paulo, São Paulo, Brazil, [6]Centre for Laser and Applications, Nuclear and Energy Research Institute, São Paulo, Brazil

Abstract Smoke particles ejected into the atmosphere from biomass burning can modify the atmospheric composition around and even far from the sources. In late winter and early spring, biomass burning emissions from inland regions can be efficiently transported to urban areas in southeastern South America, thus affecting air quality in those areas. In this study, the Weather Research and Forecasting with Chemistry model was applied in order to investigate the impact of biomass burning sources on aerosol loadings and properties over the São Paulo Metropolitan Area (SPMA), in southeastern Brazil, during the period from 19 August to 3 September 2014. The model performance was evaluated using available aerosol measurements from the Narrowing the Uncertainties on Aerosol and Climate Change in São Paulo State project. The combined application of aerosol data and Weather Research and Forecasting with Chemistry simulations made it possible to represent some of the most important aerosol properties, such as particle number concentration and cloud condensation nuclei activation, in addition to evaluation of the impact of biomass burning by analyzing a 5-day transport event, from 22 to 26 August 2014. During this transport event, differences in the average predicted $PM_{2.5}$ concentration reached 15 $\mu g/m^3$ (peaking at 20 $\mu g/m^3$ during the nighttime hours) over the SPMA, compared with 35 $\mu g/m^3$ over inland areas northwest and north of the SPMA. Biomass burning accounted for up to 20% of the baseline particle number concentration- and cloud condensation nuclei-weighted relative differences over the SPMA (2,300 and 1,400 cm^{-3}, respectively).

Key Points:
- The fully coupled WRF-Chem model was applied and evaluated for the atmosphere over the metropolitan area of São Paulo
- The WRF-Chem can reproduce observed temporal variations in meteorological conditions and chemical species
- Inclusion of biomass burning emissions improves predictions of aerosol properties

Supporting Information:
- Supporting Information S1

Correspondence to:
A. Vara-Vela,
angel.vela@iag.usp.br

Citation:
Vara-Vela, A., de Fátima Andrade, M., Zhang, Y., Kumar, P., Ynoue, R. Y., Souto-Oliveira, C. E., et al. (2018). Modeling of atmospheric aerosol properties in the São Paulo Metropolitan Area: Impact of biomass burning. *Journal of Geophysical Research: Atmospheres*, *123*, 9935–9956. https://doi.org/10.1029/2018JD028768

Received 9 APR 2018
Accepted 9 AUG 2018
Accepted article online 24 AUG 2018
Published online 12 SEP 2018

Author Contributions:
Data curation: Carlos Eduardo Souto-Oliveira, Eduardo Landulfo
Formal analysis: Maria de Fátima Andrade, Yang Zhang, Rita Yuri Ynoue
Funding acquisition: Maria de Fátima Andrade, Yang Zhang, Prashant Kumar
Investigation: Yang Zhang
Supervision: Maria de Fátima Andrade
Writing – review & editing: Maria de Fátima Andrade, Yang Zhang, Prashant Kumar, Rita Yuri Ynoue, Carlos Eduardo Souto-Oliveira

1. Introduction

Atmospheric aerosols have been the focus of numerous studies, as they play an important role concerning health impacts and climate change. Aerosol particles can attenuate solar radiation directly, by scattering and absorbing radiation—the so-called aerosol direct effect—or indirectly, by acting as cloud condensation nuclei (CCN) and thus having cloud albedo and lifetime effects—the so-called aerosol indirect effect (Hartmann et al., 2013). Research studies on aerosol effects and their implications for climate change were first compiled in the Intergovernmental Panel on Climate Change report in 1990. Since then, there have been numerous studies on the direct and indirect climatic effects of aerosols (Cai et al., 2016; Forkel et al., 2012; Scott et al., 2014; Takemura et al., 2002; Yahya et al., 2017; Zhang, 2008; Zhang et al., 2010). Most of studies of such effects in South America have focused on the Amazon rainforest, as smoke generated from biomass burning in the region can spread over significant portions of the continent, having a considerable effect on direct and indirect radiative forcing (Artaxo et al., 2013; Bevan et al., 2009; Moreira et al., 2017), as well as on human health (Alves et al., 2015, 2017; Pereira et al., 2017).

It is well recognized that the effects of aerosols on meteorological processes and air quality depend largely on the size distribution, chemical composition, mixing state, and morphology of the particles (Seinfeld et al., 2016). Organic carbon (OC) and elemental carbon (EC) have received considerable attention in recent years, among all particulate matter (PM) components typically found in urban environments, due to their complex and multiple radiative impacts on climate. Organic aerosols not only offset the warming effects caused by indirect aerosol effects but also can further build up such warming effects by chemical aging processes, affecting the atmospheric radiation balance. Oxidative aging processes can alter aerosol properties and

convert nonabsorbing organic aerosols into light-absorbing compounds, which absorb in ultraviolet and even in visible spectra, as demonstrated by Gelencser et al. (2003) in tropical clouds. Boucher et al. (2013) reviewed studies on radiative forcing by aerosols and reported that black carbon contributions offset those from organic aerosol via biomass burning emissions, resulting in an estimated mean forcing of +0.0 W/m^2 (with a range of −0.2 to +0.2 W/m^2).

There remain many uncertainties about the role that carbonaceous particles play in the composition and CCN activation of aerosols over the São Paulo Metropolitan Area (SPMA), located in the state of São Paulo, in southeastern Brazil. Oyama et al. (2016) showed that OC concentrations over the SPMA are dominated by organic aerosols from vehicular emissions, although the contributions from biogenic and biomass burning emissions are also important. The authors concluded that biomass burning accounts for 10–30% of OC and sugar cane burning accounting for 15% of mass. Biomass burning emissions may also affect the CCN activation properties of air masses arriving at SPMA. Souto-Oliveira et al. (2016) reported that high nighttime activation diameter values are associated with air masses passage over regions with active fires, which impacts negatively on CCN activation, as high activation diameter can often be attributable to low particle hygroscopicity.

Although it is well known that air pollutants from biomass burning may affect the oxidative capacity of the atmosphere in urban areas in southeastern Brazil, no major efforts have been made to investigate that effect. In fact, there have been no studies utilizing measurements of different aerosol properties in conjunction with air quality model predictions to improve understanding of aerosol emissions impacts on air quality in the region. In particular, atmospheric aerosol properties over the SPMA have not been extensively modeled, mainly due to the lack of measurements for validation of numerical simulation results. Vara-Vela et al. (2016) used the Weather Research and Forecasting with Chemistry (WRF-Chem) model to investigate the impact of on-road vehicle emissions on the formation of fine particles and found that the observed and predicted fine particle mass concentrations in the accumulation mode accounted for the majority of $PM_{2.5}$, the largest fraction of the total mass comprising OC and EC. The authors also found that the ground level O_3 concentration decreased by approximately 2% in downtown region of SPMA when the aerosol-radiation feedback was taken into account in the simulations.

The aim of the present study was to examine the main aerosol properties of the atmosphere over the SPMA, the largest metropolitan area in South America, with a special focus on quantifying the impact of biomass burning emissions on the aerosol burden. To that end, aerosol data collected in the 2014 Narrowing the Uncertainties on Aerosol and Climate Change in São Paulo State (NUANCE-SPS) campaign are compared with those obtained from three WRF-Chem simulations. In the following section the modeling framework will be introduced, including a description of emission models and the measurements used to evaluate the model results. Next, in section 3, the performance of the model will be evaluated by comparing observations with baseline model simulations. Section 4 will discuss the biomass burning contribution by analyzing a specific transport event. A summary and concluding remarks are given in section 5.

2. Description of Models, Emissions, and Observations

2.1. WRF-Chem Model and Configuration

The WRF-Chem model version 3.7.1 was employed in order to run simultaneous simulations of meteorological processes, chemistry and aerosol feedback effects on a regional scale; it is a fully coupled, online meteorology-chemistry transport mesoscale model (Grell et al., 2005; Skamarock et al., 2008).

The main physical options selected in this study included the following: the Rapid Radiative Transfer Model for General Circulation Model applications (RRTMG) scheme for longwave and shortwave radiation (Iacono et al., 2008), the Revised Mesoscale Model version 5 Monin-Obukhov scheme for surface layer (Jiménez et al., 2012), the Unified Noah land surface model for land surface (Chen & Dudhia, 2001), the single-layer urban canopy model scheme for urban model (Kusaka et al., 2001), the Yonsei University scheme for the boundary layer (Hong et al., 2006), the Multi-Scale Kain-Fritsch scheme for cumulus clouds (Zheng et al., 2016), and the Morrison two-moment scheme for microphysics (Morrison et al., 2009). In addition, the surface drag parameterization of Mass and Ovens (2010), developed to correct the high wind speed bias of the WRF model, was coupled to the boundary layer scheme to improve the predictions of wind fields. For the

chemistry, we applied the Carbon Bond mechanism CB05 (Yarwood et al., 2005) with additional chloride chemistry (Sarwar et al., 2007), coupled with the existing Modal Aerosol Dynamics model for Europe/Volatility Basis Set (MADE/VBS), as described by Ahmadov et al. (2012), to simulate concentrations of the main inorganic and organic aerosol species. The extended CB05 includes 97 species and 191 reactions, with more than 60 volatile organic compounds and 120 associated reactions. The MADE/VBS uses a three-mode aerosol representation—Aitken (< 0.1 μm), accumulation (0.1–1 μm), and coarse (> 1 μm)—and an advanced secondary organic aerosol (SOA) module based on a four-bin VBS approach with the SOA gas-particle partitioning following the theory of Pankow (Pankow, 1994a, 1994b). Nucleation processes are based on mathematical formulations described in Kulmala et al. (1998), condensation processes are based on Binkowski and Shankar (1995), and coagulation processes are based on Whitby et al. (1991) and Binkowski and Shankar (1995).

The CB05-MADE/VBS mechanism with aqueous-phase chemistry is fully coupled to existing model treatments for different aerosol-radiation-cloud feedback processes such as the aerosol direct effect on shortwave radiation, aerosol indirect effects on cloud droplet number concentration (CDNC), and cloud effects on shortwave radiation (Wang et al., 2015; Yahya, He, & Zhang, 2015). To account for the aerosol direct effect, aerosol radiative properties such as aerosol optical depth (AOD), single scattering albedo, and asymmetry factors are initially calculated based on the approach devised by Fast et al. (2006) according to the Mie theory (Mie, 1908). Those properties are then transferred to RRTMG shortwave radiation scheme in order to calculate the corresponding radiative forcing. The aerosol effects on photolytic rates for major gaseous species such as O_3 and NO_2 are linked to the Fast Troposphere Ultraviolet Visible photolysis module through the use of predicted concentrations of aerosols, including ammonium, sulfate, nitrate, OC, EC, SOAs, sea salt, and dust (Wang et al., 2015). The overall impact of aerosol indirect effects in WRF-Chem is accounted for by linking interactive aerosol modules, as implemented by Gustafson et al. (2007) and Chapman et al. (2009). After CDNC has been predicted based on the activated aerosols within the Morrison two-moment microphysics scheme, it is connected to RRTMG shortwave radiation scheme, thus affecting the calculated droplet mean radius and cloud optical depth resulting from previous changes in CDNC. In addition, feedback effects of clouds on aerosol size and composition via aqueous-phase chemistry (Sarwar et al., 2011) and wet scavenging processes (Easter et al., 2004) are treated. Aerosols are activated based on the approach described by Abdul-Razzak and Ghan (2000). Aerosols activation is based on a maximum supersaturation determined from a Gaussian spectrum of updraft velocities and bulk hygroscopicity of each aerosol compound. CCN are calculated at given maximum supersaturation values (0.02, 0.05, 0.1, 0.2, 0.5, and 1%) from the sum obtained over all lognormal particle modes (Tuccella et al., 2015). The main physics, chemistry, and emission options used in this study, as well as their corresponding references, are listed in Table 1.

2.1.1. Model Simulation Design

From August to October, during the biomass burning season in central region of South America and south of the Amazon basin, SPMA atmosphere can receive, depending on the wind direction, smoke plumes transported from those regions (Miranda et al., 2017). A case study within this season, with availability of experimental data, was performed to identify the biomass burning contribution to fine particles concentration. To that end, three sets of 18-day simulations were carried out between 17 August and 3 September 2014: one with the fire emissions module turned off (baseline simulations) and two turned on, employing different scaling factors (1 and 3) for particulate and ozone precursor emissions (sensitivity simulations). The enhancement factor of 3 is applied to produce reasonable AODs within the model and is based on previous studies conducted over South America that suggested scaling factors of 1.3 to 5 (Archer-Nicholls et al., 2015; Pereira et al., 2016). The use of the scaling factor of 3 together with the FINN baseline emissions (scaling factor of 1) provides a possible range of fire impacts estimates, through considering the uncertainties in the FINN fire emissions over South America. The need for scaling factors highlights many uncertainties involved in calculating biomass burning emissions (Archer-Nicholls et al., 2015; Ichoku et al., 2012). Emission modules and aerosol feedbacks are all incorporated into the WRF-Chem simulations.

Simulations were conducted over two nested domains at horizontal resolutions of 25 and 5 km, both with a vertical resolution of 34 layers. As shown in Figure 1, the parent domain (d01) was defined as the atmosphere over southeastern South America, whereas the nested domain (d02) focuses on the SPMA and surrounding urban areas. Both domains are designed to cover fire-prone areas, most of them located in the central west region of Brazil (northwest part of d01). Simulations at 25 km are driven by Global Forecast System 0.5°

Table 1
WRF-Chem Configurations

Attributes	WRF-Chem option
Physics	
Radiation	Longwave and shortwave RRTMG scheme (Iacono et al., 2008)
Surface layer	Revised Mesoscale Model version 5 Monin-Obukhov scheme (Jiménez et al., 2012)
Land surface	Unified Noah land surface model (Chen & Dudhia, 2001)
Urban model	Urban canopy model (Kusaka et al., 2001)
Boundary layer	Yonsei University scheme (Hong et al., 2006)
Cumulus clouds[a]	Multiscale Kain-Fritsch scheme (Zheng et al., 2016)
Cloud microphysics	Morrison two moment (Morrison et al., 2009)
Chemistry	
Gas phase	Modified CB05 with updated chlorine chemistry (Sarwar et al., 2007; Yarwood et al., 2005) implemented by Wang et al. (2015)
Aqueous phase	Sarwar et al. (2011)
Aerosol	MADE/VBS (Ahmadov et al., 2012)Modal (3): Aitken (<0.1 μm), accumulation (0.1–1 μm), and coarse (>1 μm)four-bin VBS framework with aging
Aerosol activation	Abdul-Razzak and Ghan (2000)Internal mixing state with hygroscopicity parameters for OC, k_{OC} = 0.14, and for BC, $k_{BC} = 10^{-6}$
Photolysis	Fast Troposphere Ultraviolet Visible (Tie et al., 2003)
Emission sources	
Anthropogenic	HTAPv2.2 (Janssens-Maenhout et al., 2015) and Andrade et al. (2015)[b]
Biogenic	Model of Emissions of Gases and Aerosols from Nature (Guenther et al., 2006)
Fire	FINN (Wiedinmyer et al., 2011)
Plume rise	Freitas et al. (2007)
Dust	Jones and Creighton (2011)
Sea salt	Gong et al. (1997)

Note. WRF-Chem = Weather Research and Forecasting with Chemistry; MADE = Modal Aerosol Dynamics model for Europe; VBS = Volatility Basis Set; BC = boundary condition; OC = organic carbon; RRTMG = Rapid Radiative Transfer Model for General Circulation Model applications; HTAPv2.2 = Hemispheric Transport of Air Pollution version 2.2.
[a]Parent domain only. [b]Nested domain only.

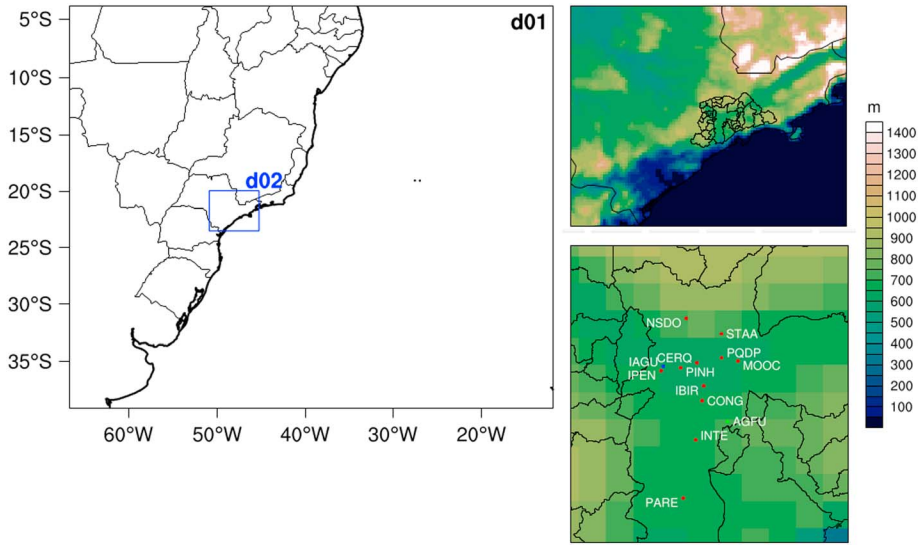

Figure 1. The two nested domains for Weather Research and Forecasting-Chem modeling. The parent domain (d01) includes the southeastern region of South America, whereas the nested domain (d02) covers the SPMA and surrounding urban areas. The zoom-in maps for d02 show the Weather Research and Forecasting topography (top right) and the location of all measurement sites within the São Paulo Metropolitan Area (bottom right). Red dots represent CETESB sites, whereas the blue and green dots represent, respectively, the locations of the Narrowing the Uncertainties on Aerosol and Climate Change in São Paulo State sampling campaigns and Institute of Astronomy, Geophysics and Atmospheric Sciences of the University of São Paulo's climatological station.

Table 2
Simulation Design and Evaluation Periods

Attributes	Parent domain	Nested domain
Simulation period	17 August to 3 September 2014	17 August to 3 September 2014
Coverage	Southeastern South America	Southeastern part of the state of São Paulo
Horizontal resolution	25 km	5 km
Vertical resolution	34 layers from surface to 50 hPa (≈20.5 km)	34 layers from surface to 50 hPa (≈20.5 km)
Baseline simulation	Meteorological ICs/BCs from GFS 0.5 model; chemical ICs/BCs from MOZART-4/GEOS-5 model; fire emission module turned off; aerosol feedbacks turned on	Meteorological and chemical ICs/BCs[a] from the 25-km baseline simulation; fire emission module turned off; aerosol feedbacks turned on; denoted as BASE for simplicity
Biomass burning sensitivity simulation	Meteorological ICs/BCs from GFS 0.5 model; chemical IC and BC from MOZART-4/GEOS-5 model; all emission modules[b] turned on; aerosol feedbacks turned on; FINN particulate and ozone precursor emissions scaled by a factor of 1	Meteorological and chemical ICs/BCs[a] from the 25-km sensitivity simulation; all emission modules[b] turned on; aerosol feedbacks turned on; FINN particulate and ozone precursor emissions scaled by a factor of 1; denoted as BBE for simplicity
Threefold-biomass burning sensitivity simulation	Meteorological ICs/BCs from GFS 0.5 model; chemical IC and BC from MOZART-4/GEOS-5 model; all emission modules[b] turned on; aerosol feedbacks turned on; FINN particulate and ozone precursor emissions scaled by a factor of 3	Meteorological and chemical ICs/BCs[a] from the 25-km sensitivity simulation; all emission modules[b] turned on; aerosol feedbacks turned on; FINN particulate and ozone precursor emissions scaled by a factor of 3; denoted as 3BBE for simplicity
Statistical evaluation[c]	Model performance: 19 August to 3 September 2014	Model performance: 19 August to 3 September 2014; FEC: 22–26 August 2014
Purpose	Baseline simulation for comparison to satellite measurements and inclusion of remote sources of BB	Baseline simulation for comparison to in situ and lidar measurements; differences BBE-BASE and 3BBE-BASE show impact of BB over the SPMA and surrounding urban areas

Note. IC = initial condition; BC = boundary condition; FEC = fire emission contribution (period); BB = biomass burning; MOZART = Model for Ozone and Related chemical Tracers; GEOS = Goddard Earth Observing System; SPMA = São Paulo Metropolitan Area; GFS = Global Forecast System.
[a]The ndown utility was applied to interpolate ICs/BCs provided by the 25-km simulations into the 5-km boundaries. [b]Includes anthropogenic, biogenic, fire, dust, and sea-salt aerosols. [c]The first 2 days are discarded as spin-up time.

analyses, for meteorological processes, and by Model for OZone and Related chemical Tracers version 4/Goddard Earth Observing System Model version 5 fields, for chemistry (Emmons et al., 2010; Molod et al., 2012); both called for input every 6 hr. Off-line initial conditions and boundary conditions derived from the 25-km simulations were used as input to feed 5-km simulations. The inflow boundary conditions derived from the 25-km baseline simulation that did not consider fire emissions were used in order to update the boundaries of the 5-km baseline simulation, hereafter referred to as BASE, whereas the inflow boundary conditions derived from the 25-km sensitivity simulations were used in order to update the boundaries of the 5-km sensitivity simulations, hereafter referred to as BBE and 3BBE, respectively, for the simulations with scaling factors of 1 and 3 for FINN particulate and ozone precursor emissions.

Model performance was evaluated by comparing observations with model results from the baseline simulations. Performance statistics were calculated for the period from 19 August to 3 September (the first 2 days of each simulation were considered spin-up time and were therefore discarded). In addition, spatial distributions of absolute and relative differences between BBE and BASE and between 3BBE and BASE were employed to quantify and characterize the changes in aerosol properties due to the inclusion of fire emissions. In this case, the differences are averaged over a 5-day episode from 22 to 26 August, as in this period prevailed meteorological conditions in terms of the transport of air pollutants from fire regions. Table 2 summarizes the simulation design for nested simulations, together with statistical evaluation periods.

2.2. Emissions

2.2.1. Anthropogenic Emissions

Anthropogenic emissions include seven sectors of human activities: power, industry, residential, agriculture, ground transport, aviation, and shipping. For the parent domain, emissions were taken from the Hemispheric Transport of Air Pollution version 2.2 (HTAPv2.2) emissions inventory (Janssens-Maenhout et al., 2015). The HTAPv2.2 is a compilation of different regional gridded inventories, as well as available sources based on nationally reported emission data sets for the 2000–2010 period. HTAPv2.2 emissions for South America are based on the Emissions Database for Global Atmospheric Research version 4.3 and are provided as monthly grid maps spatially distributed on a common grid with a resolution of 0.1° × 0.1° (latitude × longitude). For the nested domain, a mixture of top-down and bottom-up emissions inventories was used,

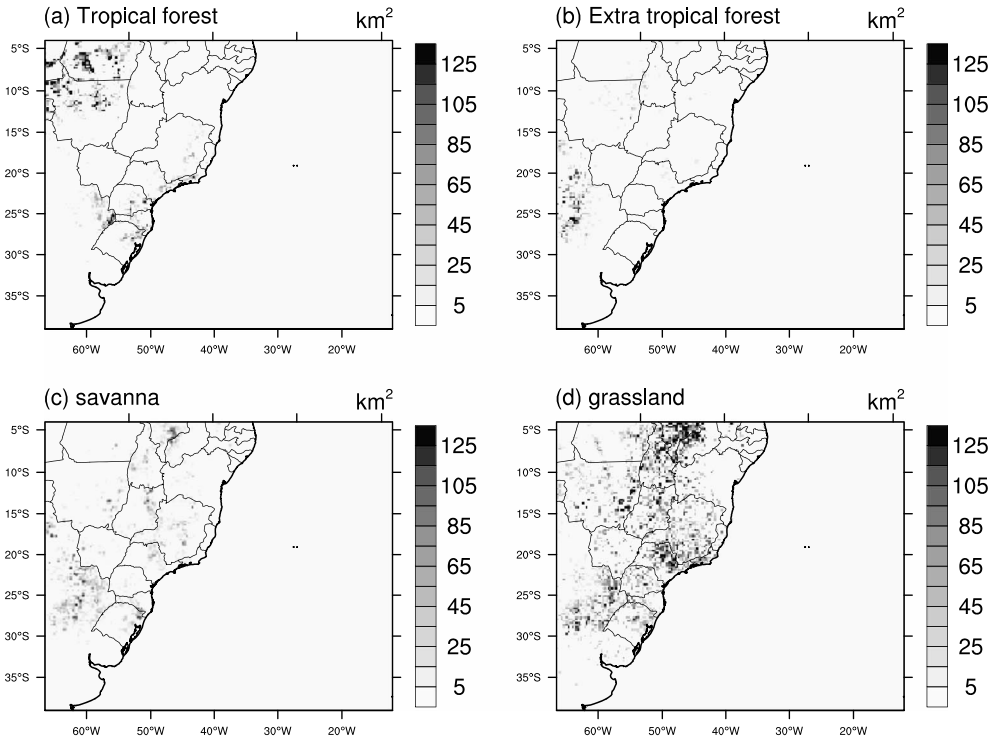

Figure 2. Spatial distribution of the total burned area for each FINN biome in the 25-km modeling domain during the period from 22 to 26 August 2014.

following the approach proposed by Hoshyaripour et al. (2016). That is, anthropogenic emissions from sectors other than ground transport (such as industrial and residential) were calculated from top-down emissions taken from the HTAPv2.2, whereas the emissions from ground transport (specifically on-road vehicles) were derived from the bottom-up transport emission model described by Andrade et al. (2015). That model combines information on emission factors for different vehicle types (motorcycles, light-duty vehicles, and heavy-duty vehicles) and different fuel types (gasohol, ethanol, ethanol-blended gasohol, and diesel) with information on road maps and vehicle counts from tunnel experiments performed in the SPMA (Andrade et al., 2015). To scale the top-down and bottom-up emissions into the 25- and 5-km modeling domains, mass-conserving emissions preprocessors anthro_emiss (Barth et al., 2015) and AAS4WRF (Vara-Vela et al., 2016, 2017) were employed, respectively. Supporting information Figure S1 shows spatial distributions of CO emission rates in both domains.

2.2.2. Fire Emissions

Fire emissions were taken from Fire INventory of the U.S. National Center for Atmospheric Research, hereafter referred to as FINN, as described by Wiedinmyer et al. (2011). The FINN provides daily emissions from open biomass burning, including wildfires, agricultural fires, and prescribed burning, on a global basis and resolution of 1 km^2. The plume rise algorithm for fire emissions was implemented in the WRF-Chem by Grell et al. (2011) and is based on the 1-D time-dependent cloud model developed by Freitas et al. (2007). This 1-D model is embedded in each grid column of the WRF-Chem grid cells containing fire spots. Lower and upper limits of the injection height are calculated based on the fire category (biome burned) provided by the fire emission model, as well as on heat flux fields inferred from the host model. Both limits are then returned to the host model and taken into account to split the total fire emissions into flaming and smoldering phases, the flaming fraction being emitted between the elevated injection heights, whereas the smoldering fraction is incorporated into the lowest model level (Archer-Nicholls et al., 2015; Freitas et al., 2007). The spatial distribution of the total burned area in the 25-km modeling domain during the period from 22 to 26 August 2014 is shown in Figure 2. For this period and modeling domain, the FINN estimates 4.9×10^{-2} Tg OC, 3.1×10^{-3} Tg EC, and 9.1×10^{-2} Tg $PM_{2.5}$.

2.2.3. Other Emissions

Biogenic emissions were calculated online using the Model of Emissions of Gases and Aerosols from Nature version 2 (Guenther et al., 2006). Based on driving variables such as ambient temperature, solar radiation, leaf area index, and plant functional type, that model estimates net terrestrial biosphere emission rates for different trace gases and aerosols with a global coverage of ≈1-km^2 spatial resolution. Dust and sea-salt aerosols were quantified online in the simulations. All emissions were considered to arise from surface with exception of fire emissions, which were added by plume rise model at the model levels previously settled on.

2.3. Measurements and Evaluation Protocols

The aerosol measurements used in this work were mostly taken from the NUANCE-SPS project. NUANCE-SPS campaigns were orchestrated by the Institute of Astronomy, Geophysics and Atmospheric Sciences of the University of São Paulo (IAG-USP) and carried out over the SPMA between 2011 and 2015. The project aimed to improve the current knowledge of the chemistry and transport processes of pollutants emitted in the SPMA and other areas of the state of São Paulo. During the most recent NUANCE-SPS campaign, performed in 2014, an extensive set of measurements of aerosol properties were obtained at 15 m above ground level, atop main IAG-USP building (23.559°S, 46.733°W; hereafter referred to as the IAGU site), which is approximately 45 km from the Atlantic Ocean.

During that NUANCE-SPS campaign, aerosol samplings were carried out during winter (dry season), from 19 August to 3 September 2014. A microorifice uniform deposit impactor (MOUDI), as described by Marple et al. (1986), was employed in order to collect mass size distributions, and a differential mobility particle sizer (DMPS), as described by Winklmayr et al. (1991), was employed in order to collect number size distributions. The rotating MOUDI collected particles in 10 different stages with nominal 50% cutoff diameters: 10, 5.6, 3.2, 1.8, 1.0, 0.56, 0.32, 0.18, 0.1, and 0.06 μm. Particles smaller than 0.06 μm were collected in a subsequent stage denominated after filter. The DMPS collected particles in 22 size bins, with diameters in the 9- to 450-nm range. Samples were collected every 12 hr with the MOUDI and every 5 min with the DMPS. A thermal-optical transmittance analysis (Sunset Laboratory Inc.; Birch & Cary, 1996) was applied to samples in order to determine the amount of EC deposited on the filters, being applied to each stage in the case of the MOUDI impactor. CCN were counted with a single-column continuous-flow streamwise thermal gradient chamber (Lance et al., 2006; Roberts & Nenes, 2005). The total polydisperse CCN number concentration is measured as a function of time and supersaturation. One measurement cycle included CCN measurements at supersaturation values of 0.2, 0.4, 0.6, 0.8, and 1.0%, each being measured for 5 min (Almeida et al., 2014). Given that DMPS and CCN data were derived from different instruments, correction factors were previously applied in order to determine the particle number concentration (PNC) spectrum in the 450- to 1,000-nm range, as well as to constrain the activated ratio (AR) to a value $\leq$1. Further details on DMPS calibration data and correction factors can be found in Souto-Oliveira et al. (2016). Vertical profiles of aerosol extinction were retrieved using a backscatter lidar system supplying vertical distributions of aerosol backscatter and extinction coefficients, obtained from elastic backscatter and Raman channels at 532 and 607 nm, respectively.

Concentrations of $PM_{2.5}$, PM_{10}, and O_3, as well as meteorological data, were obtained from the São Paulo Environmental Protection Agency monitoring network and the IAG-USP climatological station. The location of measurement sites is depicted in Figure 1 and described in supporting information Table S1. Information on precipitation and AOD derived from satellite data were considered in addition to in situ and lidar measurements throughout the evaluation of numerical simulations. Table 3 summarizes the observational data sets used for model evaluation.

During the comparison between the model results and the observations, we used statistical indices recommended for PM analyses (Boylan & Russell, 2006; Environmental Protection Agency, 2007; Zhang et al., 2006) including mean fractional bias (MFB), mean fractional error (MFE), normalized mean bias (NMB), and normalized mean error (NME), as well as other indices providing meaningful information such as mean bias (MB) and correlation coefficient (R), as defined in supporting information Table S2. In some cases, data were compared against the Global Precipitation Climatology Project (GPCP) database and against the MERGE technique (Rozante et al., 2010). For ease of model-satellite data comparison, satellite and model data were both initially regridded onto a common grid with resolution of 0.25° × 0.25° (latitude × longitude) and then averaged in time and space over the grid.

Table 3
Description of the 2014 NUANCE-SPS Aerosol Sampling Campaign Performed at the IAGU Site and Other Data Sets Included in the Model Evaluation

Database	Parameter	Sampling frequency	Sampling device
NUANCE-SPS	Particle mass concentration	12 hr	Rotating MOUDI[a]
	Particle number concentration	5 min	DMPS aerosol spectra
	CCN concentration	1 s	CCN chamber
	Aerosol extinction coefficient		Raman lidar system[b]
	EC concentration	12 hr	Sunset OC-EC analyser[c]
CETESB[d]	$PM_{2.5}$, PM_{10}, O_3, NO_2, T, RH, WS, and WD	Hourly	Various
GPCP[e]	Precipitation	Daily	
MERGE[e]	Precipitation	Daily	
MODIS[e]	AOD	Daily	

Note. T = temperature; RH = relative humidity; WS = wind speed; WD = wind direction; MODIS = Moderate Resolution Imaging Spectroradiometer. NUANCE-SPS = Narrowing the Uncertainties on Aerosol and Climate Change in São Paulo State; MOUDI = microorifice uniform deposit impactor; DMPS = differential mobility particle sizer; CCN = cloud condensation nuclei; OC = organic carbon; EC = elemental carbon.
[a]Includes aerosol mass size distribution for EC. [b]The system was set up at the USP Institute for Energy Research and Nuclear Science, which is approximately 900 m from the IAGU site. [c]PM collected on a MiniVol sampler. [d]Ambient data were taken from 11 monitoring sites (see Table S1 for details). [e]Data sets used for the evaluation of the 25-km baseline simulation.

3. Model Evaluation

Section 3 focuses on the model performance evaluation for the baseline simulations. In section 4, the results from the simulations BBE and 3BBE will be compared with those from BASE, in order to assess the impacts of fire emissions on air quality and on aerosol properties.

3.1. Meteorology

To study the impact that the long-range transport of fire emissions may have on aerosol particles in the SPMA, meteorological conditions, especially wind speed and wind direction, were analyzed. Comparisons between the observed and predicted hourly variations for 2-m temperature, 2-m relative humidity, 10-m wind speed, and 10-m wind direction (see supporting information Figure S2) show that the model performs well in terms of trends. However, it tends to underpredict temperature and relative humidity, the average MB over all sites being 0.01 °C and 2%, whereas it overpredicts wind speed, the average MB being 0.57 m/s. Wind direction is predicted to be more easterly compared with the observed fields, southeasterly winds largely dominated by the influence of sea breezes. Individual calculations of performance statistics are presented in supporting information Table S3.

Although winds were not generally favorable for the transport of air pollutants from fire areas, shifts in wind direction, foremost from southeasterly to northwesterly, over a 5-day period (from 22 to 26 August) favored such transport and thereby the enhancement of aerosol loadings into the SPMA. In another favorable event (from midday 31 August to midnight 1 September), wind speeds increased to 8 m/s. However, despite the fact that, during that short period, the number of fire events was proportionally higher in comparison with the total study period, there were multiple precipitation events related to the passage of a low-pressure system that spread rapidly over the SPMA, contributing significantly to the removal of gases and particles. Except during those two periods, the winds were not favorable for transport from fire regions. There were precipitation events on some days within the second half of the study period (27 August to 3 September 2014). Precipitation predictions agreed well with ground- and satellite-based measurements. The model evaluation for the 25-km baseline simulation shows good domain mean performance statistics with MBs and NMBs within 0.7 mm/day (0.4 mm/day against the MERGE data and 0.7 mm/day against the GPCP database) and within 30% (17% against the MERGE data and 30% against the GPCP database), respectively. The differences are attributable to different spatial coverage and composition and may have led to bias compensation. Figure S3 in the supporting information compares punctual precipitation data obtained from the IAG-USP climatological station with the amounts of rainfall under the corresponding points for the 5-km modeling domain and in the MERGE data (see Table S3 in the supporting information for performance statistics).

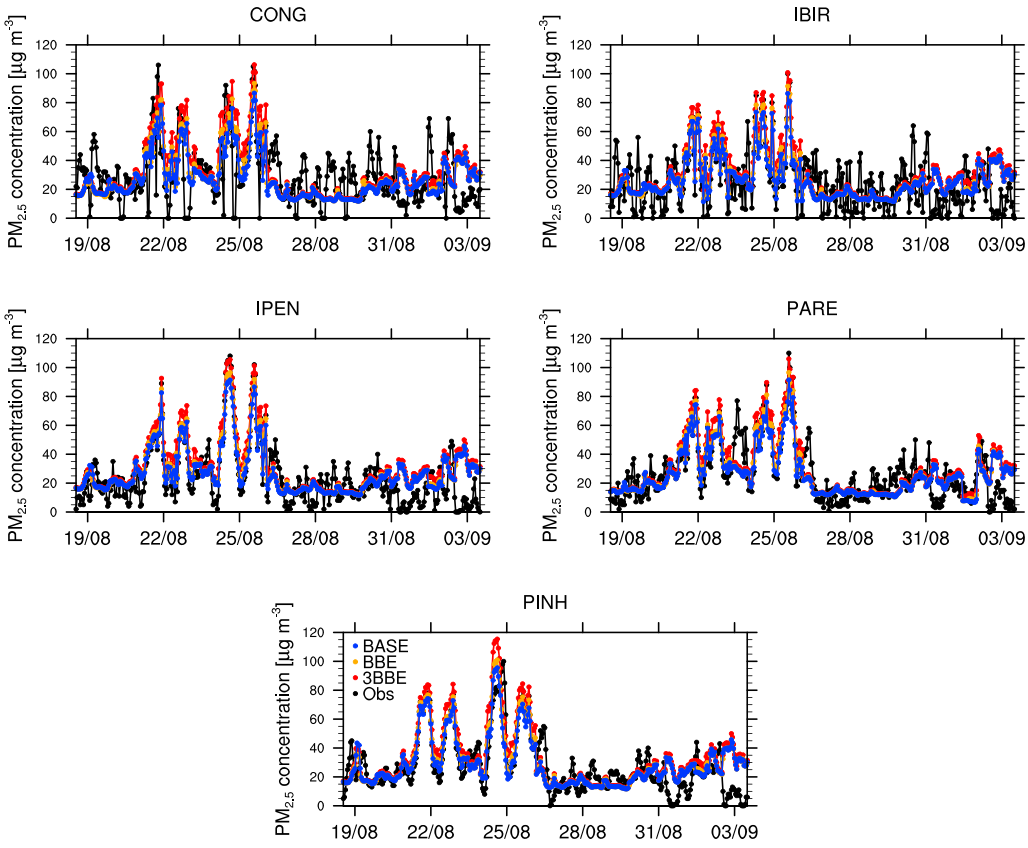

Figure 3. Hourly variations in $PM_{2.5}$ concentrations at five CETESB monitoring sites during the period from 19 August to 3 September 2014, showing observed values (black dots) and predicted values (blue, orange, and red dots, respectively, for the simulations BASE, BBE, and 3BBE).

3.2. Chemical Concentrations

Figures 3–5, respectively, compare the observed near-surface $PM_{2.5}$, PM_{10}, and O_3 concentrations with the concentrations predicted in the BASE simulation (blue dots in the figures). During the period from 22 to 26 August, characterized by the influence of biomass burning smoke transported from inland regions, observations showed a strong day-to-day and diurnal variability in pollutant levels, with concentrations up to 110, 240, and 210 $\mu g/m^3$, respectively, for $PM_{2.5}$, PM_{10}, and O_3. The model tracked the temporal variations in the concentrations of those pollutants reasonably well during this period when there were no precipitation events. However, significant discrepancies during the second half of the study period (27 August to 3 September 2014), and attributable to changes in meteorological conditions, especially cloud cover and rain, were also observed. In general, underestimation of concentrations is related to either inaccurate meteorological predictions or underestimation of the emissions, or a combination of both. For the concentrations of $PM_{2.5}$, PM_{10}, and O_3, the average MBs were 1.02, −2.87, and −5.32 $\mu g/m^3$, respectively, and the average NMBs were 4.30, −4.79, and −12.45%, respectively. Individual indices are available in supporting information Table S4. Each point on the scatter plots in Figure 6, displayed with a marker (PM variable) and a color (monitoring site), represents the PM model performance in terms of NMB and NME, the panels (a) and (d) showing the results from the BASE simulation for the periods from 22 August to 3 September 2014 and from 22 to 26 August 2014, respectively. Comparisons between the observed and predicted concentrations of EC at the IAGU site are shown in supporting information Figure S5. The considerable underprediction of EC might be due to underestimates of EC emissions in the fire emissions inventory. As reported by Pereira et al. (2016), the FINN tends to underestimate the smoke emission loading in the eastern portion of the Amazon rainforest.

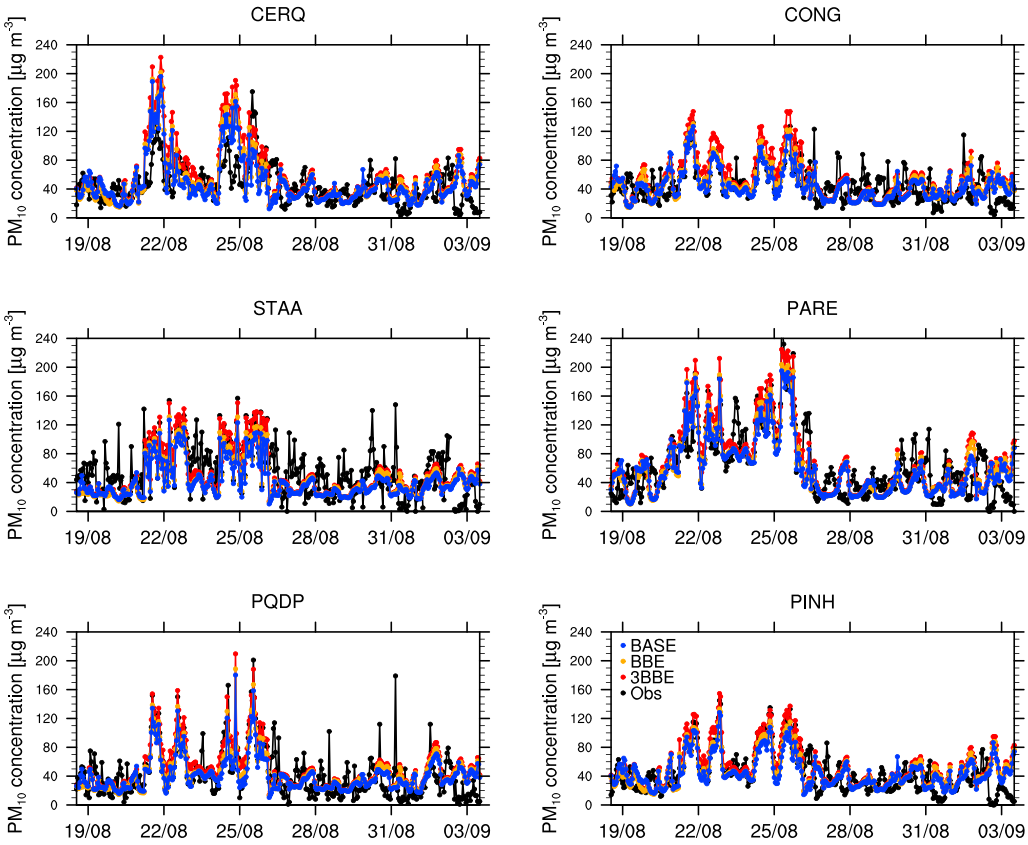

Figure 4. Hourly variations in PM_{10} concentrations at six CETESB monitoring sites during the period from 19 August to 3 September 2014, showing observed values (black dots) and predicted values (blue, orange, and red dots, respectively, for the simulations BASE, BBE, and 3BBE).

3.3. Size Distribution, OC-EC Contribution, and Optical Properties

Figures 7 and 8 depict the predicted particle mass and number concentrations, respectively, using available observations. For comparison purposes, the particle masses in each MOUDI bin were grouped into the MADE modes according to their size limits. In addition, due to limited measurements of mass size distribution, the observed and predicted particle mass concentrations were compared based on the MOUDI sampling period, which included only 1 day within the fire emission contribution period prior to the shift in meteorological conditions. On the basis of the WRF-Chem nomenclature, nu0 and ac0 are used here to refer to PNC in the Aitken and accumulation modes, respectively. The comparison of particle number data from the model against DMPS data revealed overall good agreement in terms of temporal evolution (see the left panels in Figure 8). However, some peaks attributed to very specific small-scale features, mainly in the second half of the study period, were not fully captured by the model. The predicted PNC showed lower variability than did the observed PNC (see the bottom right panel in Figure 8), with PNC MB values of −1,133.67 and −1,926.52 cm^{-3}, respectively, for the periods from 19 August to 3 September 2014 (ESP) and from 22 to 26 August 2014 (FEC; see Table 4). The differences between the predicted and observed PNC values are attributable in large part to uncertainties in the estimation of nucleation rates and of primary emissions of aerosol particles, the latter considered to be the key factor for CCN production within the planetary boundary layer (PBL), as described by Tuccella et al. (2015) and Spracklen et al. (2006).

The model evaluation for $PM_{2.5}$ chemical composition, in terms of light absorption at ultraviolet and visible wavelengths, focused only on the two most important aerosol components: EC (observed and predicted) and OC (predicted only). The predicted OC and EC composed the largest fraction of the total PM_1 mass at the IAGU site, with individual contributions of 49.2% and 9.6%, respectively, compared with only 8.8% for the observed EC. In addition, the predicted SOAs at the IAGU site were found to correspond to 24% of the

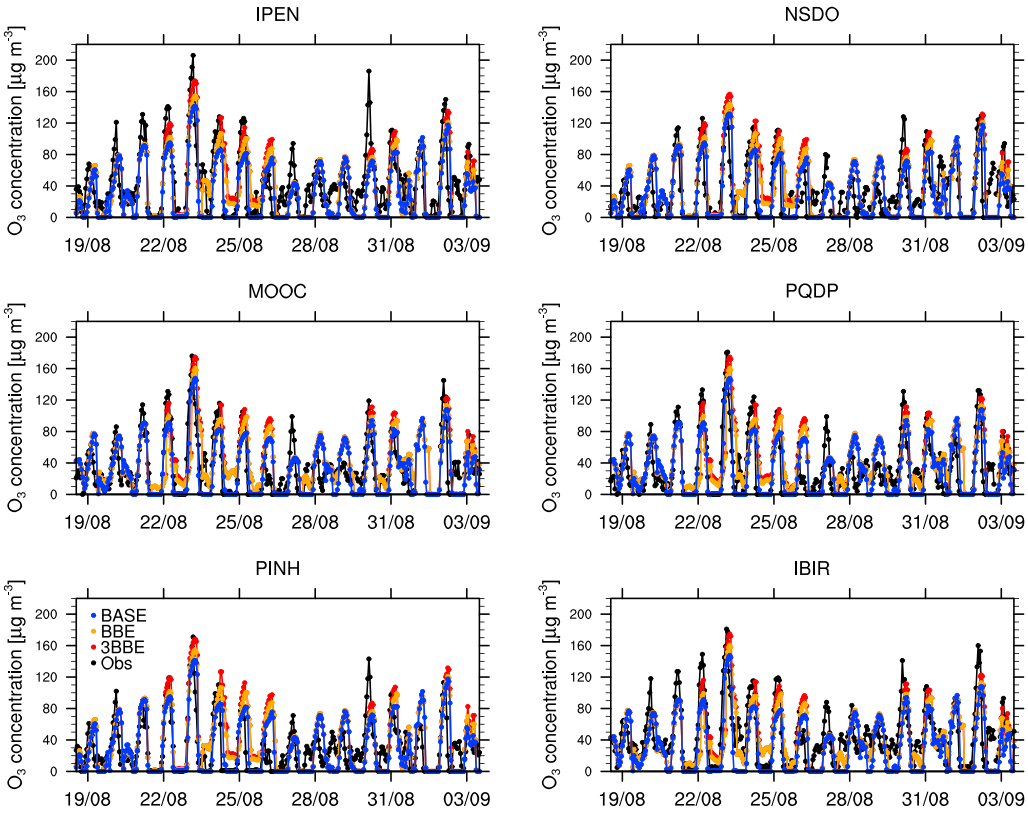

Figure 5. Hourly variations in O_3 concentrations at six CETESB monitoring sites during the period from 19 August to 3 September 2014, showing observed values (black dots) and predicted values (blue, orange, and red dots, respectively, for the simulations BASE, BBE, and 3BBE).

predicted OC (11.8% of the total PM_1 mass). A previous study, also conducted over the SPMA (Vara-Vela et al., 2016), reported that the predicted SOAs accounted for 17% of the OC mass. Although those proportions represent average contribution during August for different but proximal years (2012 and 2014), the approximately 7% higher SOA contribution obtained in this study is attributable to the use of a

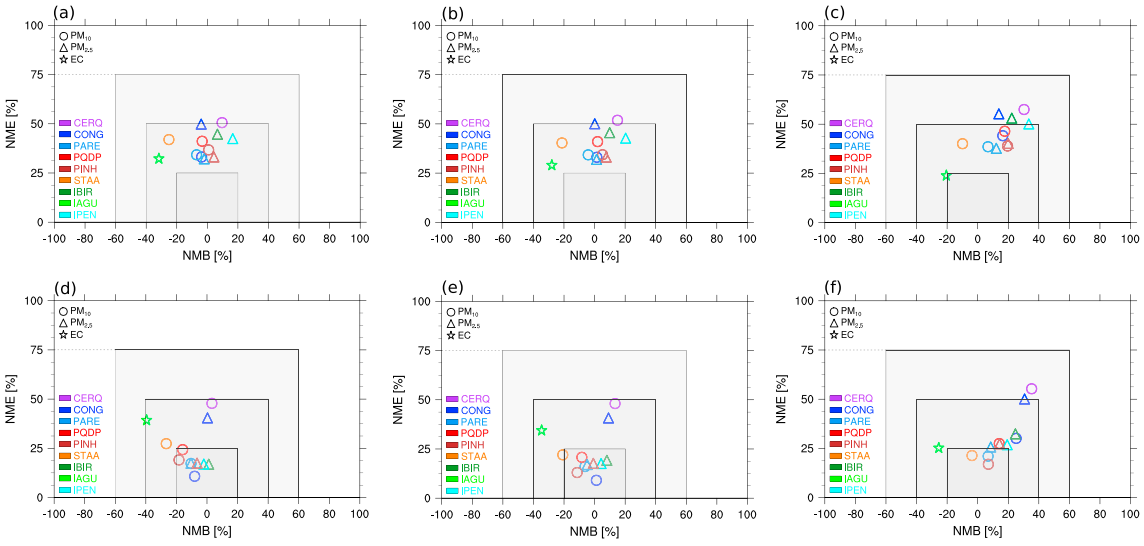

Figure 6. PM soccer plots (NMB vs. NME) for the simulations BASE (a, d), BBE (b, e), and 3BBE (c, f) during the periods from 19 August to 3 September 2014 (a–c) and from 22 to 26 August 2014 (d–f). NMB = normalized mean bias; NME = normalized mean error; PM = particulate matter; EC = elemental carbon.

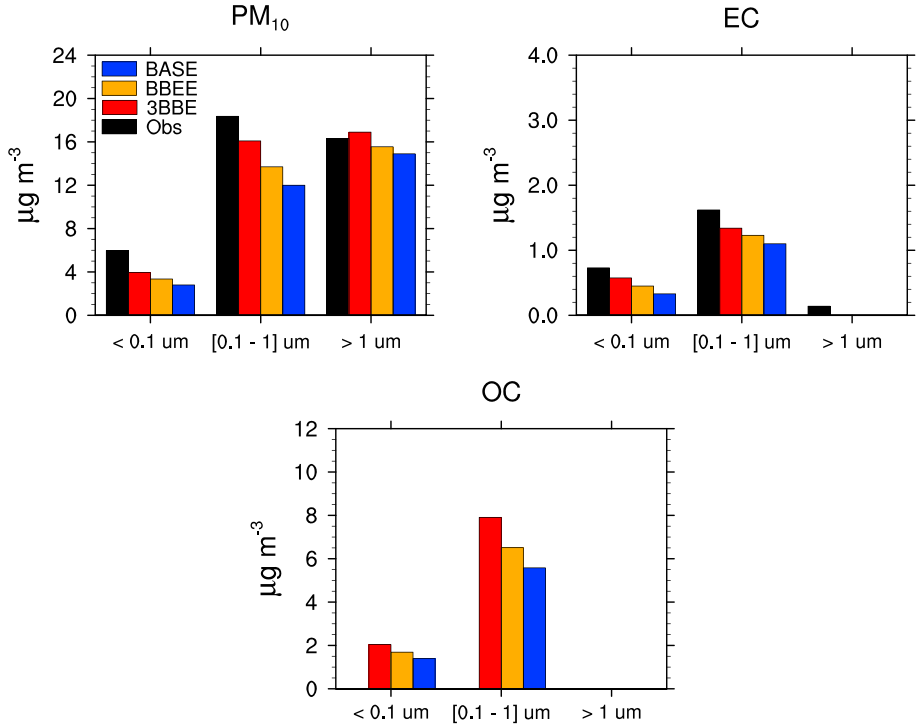

Figure 7. Observed and predicted particle mass concentration of average PM_{10} (top left) and EC (top right), together with the predicted average OC (bottom). The mass concentrations in each MOUDI bin were first grouped according to the three modes used in the MADE aerosol module, after which they were averaged for the MOUDI sampling period (8 days during the study period). PM = particulate matter; EC = elemental carbon; OC = organic carbon; MOUDI = microorifice uniform deposit impactor.

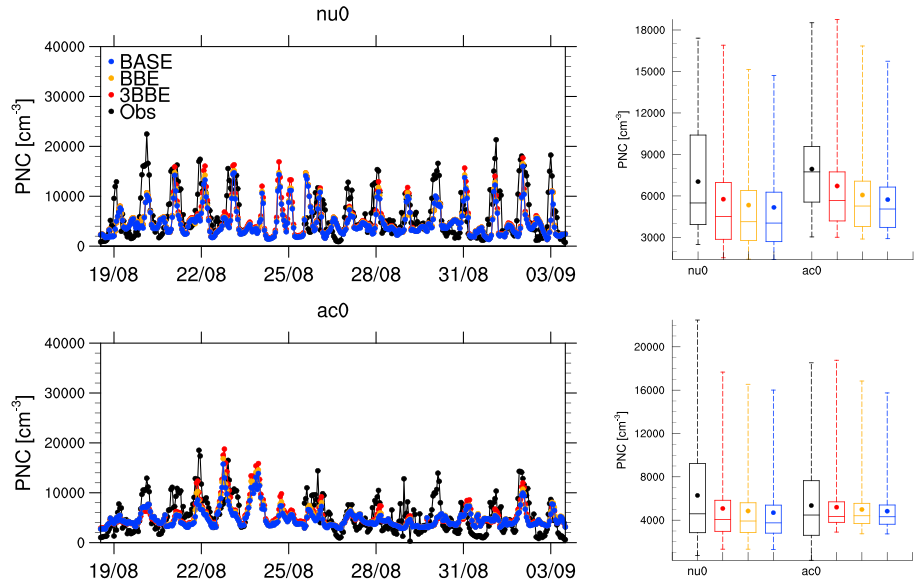

Figure 8. Time series (left) and box whisker plots (right) of PNC, in the Aitken mode (nu0) and in the accumulation mode (ac0), at the IAGU site during the periods from 22 to 26 August 2014 (top right) and from 19 August to 3 September 2014 (bottom right), showing observed values (in black) and predicted values (in blue, orange and red, respectively, for the simulations BASE, BBE, and 3BBE). PNC = particle number concentration.

Table 4
WRF-Chem Performance Statistics for PNC (ac0), $CCN_{1\%}$, and $AR_{1\%}$ at the IAGU Site

Variables	Index	BASE (ESP)	BBE (ESP)	3BBE (ESP)	BASE (FEC)	BBE (FEC)	3BBE (FEC)
PNC	SD_{Obs}	4,012.10	4,012.10	4,012.10	3,657.51	3,657.51	3,657.51
	SD_{Sim}	2,341.40	2,410.26	2,892.99	3,024.20	3,229.41	3,664.66
	R	0.49	0.50	0.52	0.44	0.46	0.49
	RMSE	3,733.46	3,634.11	3,493.02	4,297.82	4,211.12	4,019.19
	MB	−1,133.67	−985.87	−806.83	−1,926.52	−1,644.02	−1,105.37
$CCN_{1\%}$	SD_{Obs}	1,519.12	1,519.12	1,519.12	1,575.87	1,575.87	1,575.87
	SD_{Sim}	1,006.62	1,072.29	1,219.87	913.19	986.23	1,131.71
	R	0.37	0.36	0.39	0.38	0.38	0.40
	RMSE	1,605.32	1,615.98	1,637.21	2,071.75	2,003.35	1,857.88
	MB	−626.50	−607.47	−435.99	−1,230.86	−1,073.58	−650.54
$AR_{1\%}$	SD_{Obs}	0.16	0.16	0.16	0.16	0.16	0.16
	SD_{Sim}	0.14	0.14	0.15	0.16	0.16	0.17
	R	0.39	0.42	0.41	0.40	0.42	0.42
	RMSE	0.18	0.17	0.17	0.17	0.17	0.18
	MB	−0.05	−0.04	−0.03	−0.02	−0.02	−0.001

Note. ESP = entire study period; FEC = fire emission contribution (period); SD_{Obs} = observed standard deviation; SD_{Sim} = simulated standard deviation; R = correlation coefficient; RMSE = root-mean-square error; MB = mean bias; WRF-Chem = Weather Research and Forecasting with Chemistry; PNC = particle number concentration; CCN = cloud condensation nuclei; AR = activated ratio.

nontraditional SOA model rather than a traditional SOA model, such as those used by Vara-Vela et al. (2016) and Tuccella et al. (2012), together with the use of an extended and updated biogenic emissions model.

Model results for the 25-km baseline simulation are in good domain-wide agreement with the Moderate Resolution Imaging Spectroradiometer AOD data (R = 0.55; MB = −0.08; NMB = −0.47). On the basis of a spatial average, the largest AOD underestimations were for the atmosphere over the central west region of Brazil (see supporting information Figure S6), indicating that particle loadings are underestimated over this region. Biomass burning events are quite common in the central west region of Brazil and represent the dominant aerosol sources during the burning season (August to October), as reported by Hoelzemann et al. (2009). However, comparisons between the data derived from the BASE simulation and those of the two available lidar aerosol extinction profiles show that the model failed to simulate the vertical structure of aerosols, being able to produce only some of the aerosol layering observed between 12:00 and 13:00 UTC on 26 August (left panel in Figure 9), prior to the shift toward unfavorable conditions in terms of precipitation and transport from fire regions. Similarly, the higher-resolution model simulation underestimated the magnitude of extinction coefficients and thus that of the AOD.

3.4. CCN

Aerosols can be activated depending on the supersaturation, aerosol composition, and particle size. Although the relative importance of these parameters may vary greatly in different environments and locations, there is general agreement that the activation of CCN at a given supersaturation depends primarily on the particle size, followed by the chemical composition and mixing state (Che et al., 2017). In the present study, activation of CCN was assessed by comparing the observed and predicted AR values at supersaturations of 0.2% and 1.0%. The AR was calculated, with PNC integrated over bins and modes, as follows:

$$\mathrm{AR} = \frac{\mathrm{CCN}}{\mathrm{PNC}} \tag{1}$$

with a particle diameter ≤ 1 μm. The AR, thus calculated, was employed for determining the efficiency of aerosol particles in acting as CCN, following the examples of previous studies of the atmosphere over the SPMA conducted by Almeida et al. (2014) and Souto-Oliveira et al. (2016). Time series and box whisker plots of CCN concentrations at the IAGU site are shown in the Figure 10, and Figure 11 shows the same for ARs. The CCN comparisons show that the model represented the spread of CCN relatively well at both supersaturations, confirming the importance of supersaturation in the magnitude of the CCN activation. Underestimation of the predicted CCN was directly related to an underestimation of the predicted PNC. Global and regional

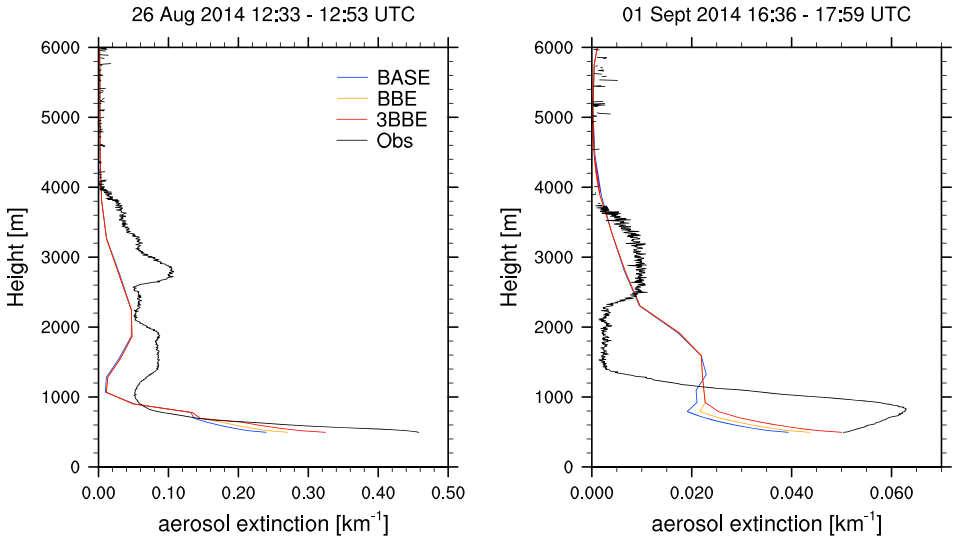

Figure 9. Average observed (Obs) profiles of aerosol extinction obtained by lidar at the Institute for Energy Research and Nuclear Science, in the city of São Paulo (black lines), compared with the average profiles obtained from the simulations BASE, BBE, and 3BBE (blue, orange, and red lines, respectively). The panels on the left and right show the comparisons of averaged profiles between 12:00 and 13:00 UTC on 26 August (no rain conditions) and between 16:00 and 18:00 UTC on 1 September (rain conditions), respectively. Winds from fire regions were favorable during both observation periods.

modeling studies have suggested that CCN production depends largely on the primary emission of aerosol particles (Merikanto et al., 2009; Spracklen et al., 2006; Tuccella et al., 2015). In the present study, the observed and predicted CCN activation were more significant at 1% supersaturation. In addition, depending on the aerosol composition, particle hygroscopicity may or not catalyze the activation of CCN. In the WRF-Chem, CCN activation depends on the volume-weighted average hygroscopicity of each aerosol component (e.g., salt, sulfate, nitrate, ammonium, and SOAs, which are the aerosol particles that react readily with water).

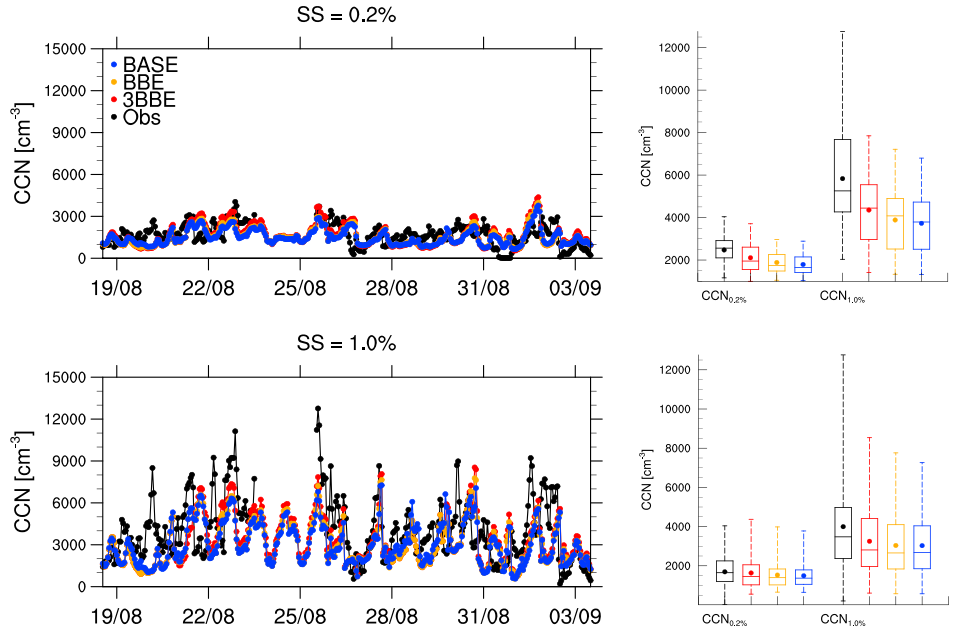

Figure 10. Times series and box whisker plots of CCN at the IAGU site during the periods from 22 to 26 August 2014 (top right) and from 19 August to 3 September 2014 (bottom right), showing observed values (in black) and predicted values (in blue, orange, and red, respectively, for the simulations BASE, BBE, and 3BBE). CCN = cloud condensation nuclei; SS = supersaturation.

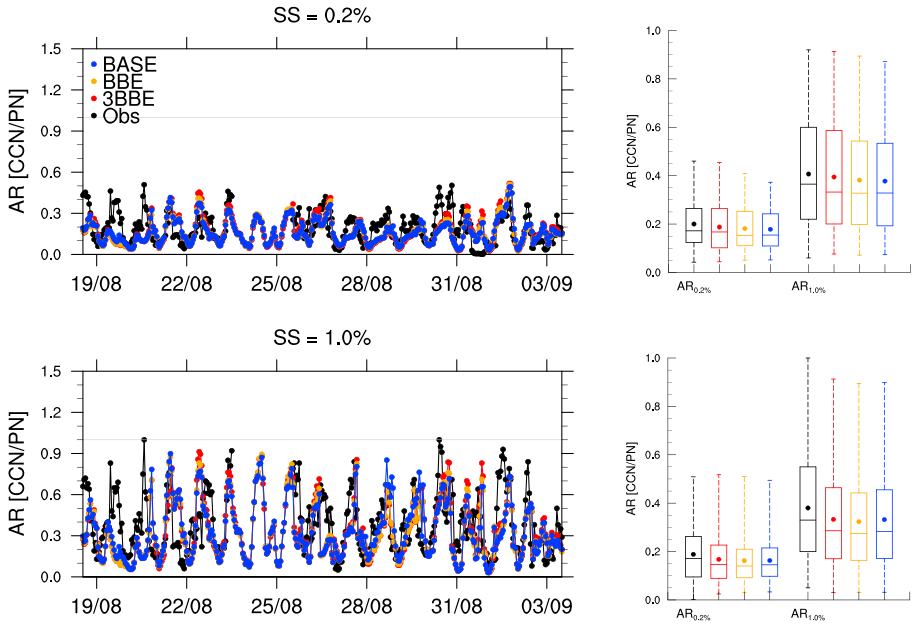

Figure 11. Times series and box whisker plots of ARs at the IAGU site during the periods from 22 to 26 August 2014 (top right) and from 19 August to 3 September 2014 (bottom right), showing observed values (in black) and predicted values (in blue, orange and red, respectively, for the simulations BASE, BBE, and 3BBE). AR = activated ratio; CCN = cloud condensation nuclei; PN = particle number; SS = supersaturation.

Although the model underestimates the CCN and PNC concentrations, the predicted AR values agreed well with the observations throughout the study period, with similar observed and predicted interquartile ranges (see the right panels in Figure 11). This is due to the fact that both of the terms on the right-hand side of equation (1) were underestimated by similar scale factors relative to their corresponding observed values. The observed AR peaks that were not fully captured by the model are attributable to PNC-related local-scale features. Table 4 summarizes the observed and predicted standard deviations, correlation and MB of PNC (ac0), $CCN_{1\%}$, and $AR_{1\%}$.

4. Impacts of Biomass Burning Emissions

4.1. Meteorology

Figure S2 in the supporting information shows that there were slight differences between the BBE and BASE simulations in terms of temperature, relative humidity, and winds, which may be related to the feedback effects that biomass burning aerosols have on meteorological processes. Aerosols affect those processes through changes in radiation and PBL dynamics. Previous studies have suggested, however, that the interactions between meteorological processes and chemical species can be significant during strong air pollution episodes such as wildfires or dust events (Chen et al., 2014; Kong et al., 2015). Yahya, Wang, et al. (2015) showed that including chemical feedbacks into meteorology helps reduce biases in simulated meteorological variables, in particular, shortwave radiation.

4.2. Chemical Concentrations

Figures 3–5 show the impact of fire emissions on near-surface $PM_{2.5}$, PM_{10}, and O_3 concentrations, respectively. Focusing on the fire emission contribution period, we found that fire emissions increased the concentration of fine particles and O_3, reducing the MB and NMB for $PM_{2.5}$, respectively, from -1.69 μg/m^3 and -3.51% for BASE to 1.18 μg/m^3 and 3.14% for BBE but increasing them to 6.75 μg/m^3 and 17.51% for 3BBE (which is still within the range of NMBs expected for good performance; see Table 5). However, most of the pairs (NMB and NME) for $PM_{2.5}$ and PM_{10} were more clustered around the zero lines when compared to those from the entire study period (see Figure 6). Larger contributions of fire emissions to the maximum O_3 and $PM_{2.5}$ concentrations may be explained by the transport of such air pollutants from fire regions (during the day for O_3 and during the night for fine particles), as well as by additional in situ

Table 5
$PM_{2.5}$ Performance Statistics for WRF-Chem Predictions at all Sites

Index	BASE (ESP)	BBE (ESP)	3BBE (ESP)	BASE (FEC)	BBE (FEC)	3BBE (FEC)
SD_{Obs}	20.19	20.19	20.19	23.30	23.30	23.30
SD_{Sim}	15.61	16.86	19.61	18.50	19.67	21.85
R	0.70	0.71	0.70	0.81	0.80	0.79
RMSE	14.38	14.40	16.05	13.19	13.41	16.61
MB	1.02	1.97	5.29	−1.69	1.18	6.75
MFB	18.34	20.59	26.84	4.56	10.78	22.50
MFE	51.33	51.66	53.62	28.97	30.39	36.57
NMB	4.30	7.87	18.34	−3.51	3.14	17.51
NME	40.44	40.67	46.26	21.82	22.46	30.45

Note. ESP = entire study period; FEC = fire emission contribution (period); SD_{Obs} = observed standard deviation; SD_{Sim} = simulated standard deviation = RMSE: root-mean-square error; MB = mean bias; MFB = mean fractional bias; MFE = mean fractional error; NMB = normalized mean bias; NME = normalized mean error; WRF-Chem = Weather Research and Forecasting with Chemistry.

formation due to changes in precursor concentrations. In addition, nighttime O_3 concentrations deviated further from (above) the observations, indicating insufficient titration of O_3 by nitrogen oxides (NO_x). Positive O_3 MB and NMB values of 7.84 μg/m^3 and 23.20%, respectively, for BBE and of 12.72 μg/m^3 and 35.84%, respectively, for 3BBE, were closely related to large positive nighttime biases in relation to the fire emission contribution period. In this case, insufficient titration reactions are related to underprediction of NO_x emissions from biomass burning regions. The level of NO_x can influence O_3 mixing ratios through titration chemistry during the night and in the early morning hours (Yahya, He, & Zhang, 2015). Comparisons between the observed and predicted concentrations of NO_2 at four CETESB sites are shown in supporting information Figure S4. In comparison with the fire emission contribution period, the period as a whole showed less noticeable performance improvements for $PM_{2.5}$ and O_3, with increases in the $PM_{2.5}$ MB and NMB from 1.02 μg/m^3 and 4.26%, respectively, for BASE to 1.87 μg/m^3 and 7.37% and to 5.09 μg/m^3 and 17.94%, respectively, for BBE and 3BBE. Positive $PM_{2.5}$ bias increases in both periods are related not only to the inclusion of fire emissions in the simulations, but mainly to baseline bias compensation (see Figure 3).

To identify and quantify the maximum local and remote contributions with greater accuracy, we calculated time-averaged distributions of EC, OC, and $PM_{2.5}$ on the basis of the five daily $PM_{2.5}$ peaks within the fire emission contribution period. Figure 12 shows the temporal mean spatial distributions of absolute and relative differences of the predicted daily maximum near-surface concentrations of EC (a–d), OC (e–h), and $PM_{2.5}$ (i–l). In line with the differences in fire emissions, the 3BBE simulation yielded higher PM impacts for the most part of the domain than did the BBE simulation. In addition, the model revealed that the largest fire impacts on $PM_{2.5}$, with relative differences of nearly 27% (12 μg/m^3) and 72% (35 μg/m^3), respectively, for BBE

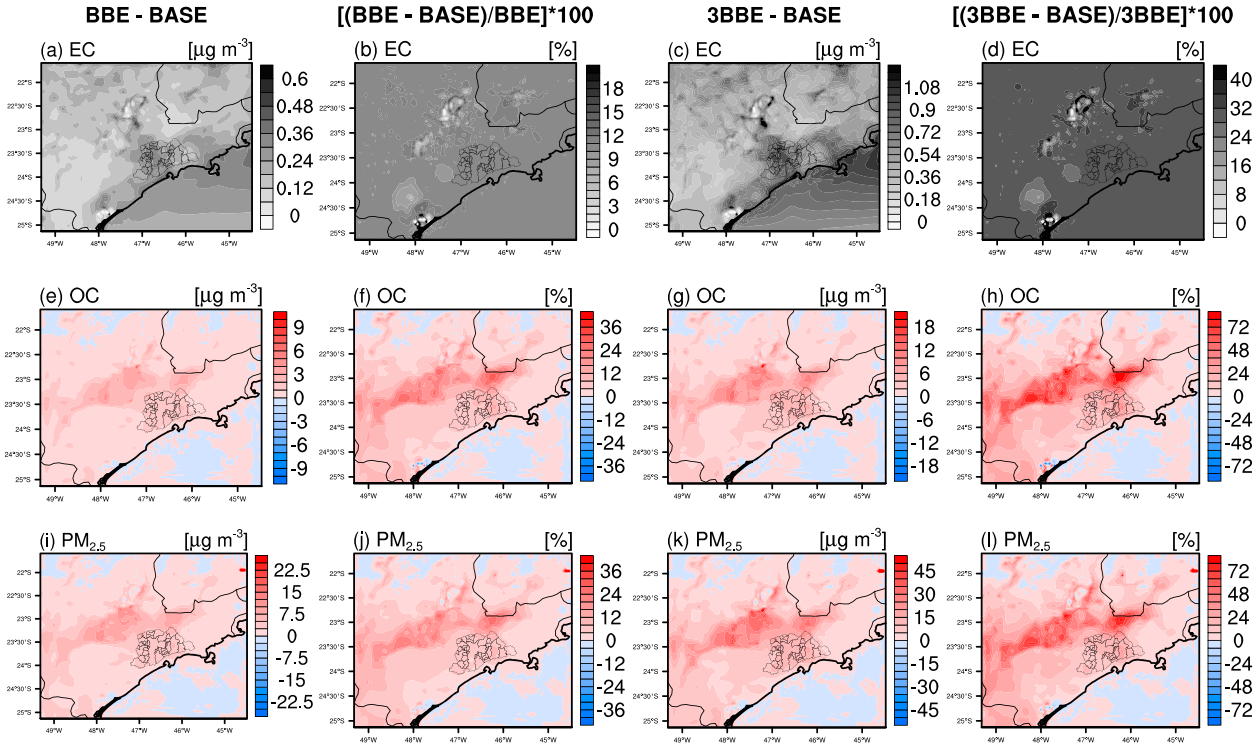

Figure 12. Temporal mean spatial distributions of absolute and relative differences of the predicted daily maximum near-surface concentrations of EC (a–d), OC (e–h), and $PM_{2.5}$ (i–l) during the fire emission contribution period, from 22 to 26 August 2014. EC = elemental carbon; OC = organic carbon; PM = particulate matter.

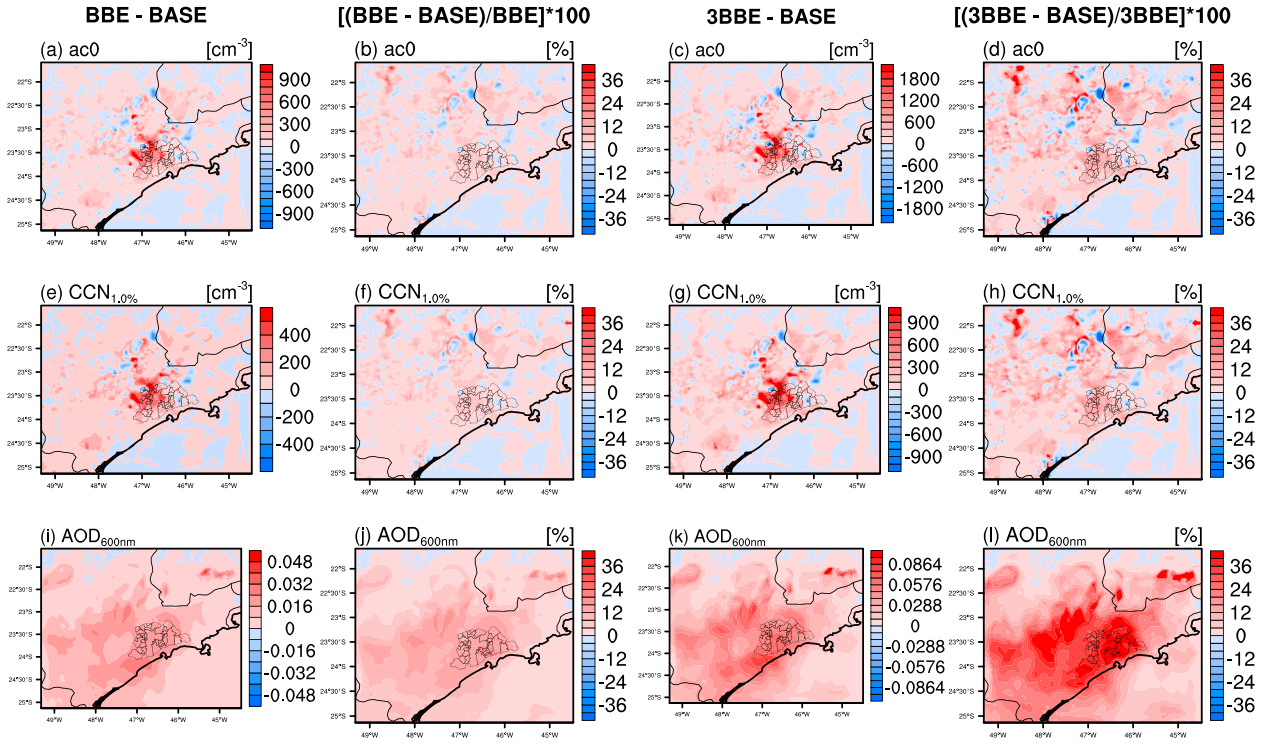

Figure 13. Temporal mean spatial distributions of absolute and relative differences of the predicted daily maximum concentrations of ac0 (a–d), $CCN_{1.0\%}$ (e–h), and both at surface- and column-integrated AOD_{600nm} (i–l) during the fire emission contribution period, from 22 to 26 August 2014. CCN = cloud condensation nuclei; AOD = aerosol optical depth.

and 3BBE, were northwest and north of the SPMA, within the inland portion of the state (see the deep red stain in Figures 12j and 12l). The larger contributions of fire emissions to $PM_{2.5}$ loadings in this region are likely due to two factors. First, a large number of fire spots were identified within the region throughout the fire emission contribution period (see Figure 2), leading to an increase in aerosol concentrations either directly, through the emission of aerosol particles (e.g., primary organic aerosols) or indirectly, via secondary formation due to the complex interactions between gases and aerosols released from fires and from vegetation; and second, long-range transport of pollutants from fire events occurring far inland, particularly those occurring in the northwest strip (relative to the area of interest), from where the winds had persistently blown toward the southeastern part of the state.

4.3. Size Distribution, OC-EC Contribution, and Optical Properties

As shown in Figure 8, the maximum differences in the predicted PNC (BBE-BASE and 3BBE-BASE for PNC) of aerosol particles in the accumulation mode occurred during the fire emission contribution period, which was characterized by the transport of air pollutants from fire regions. However, the slight increases in PNC on some days during the second half of the period were found to be caused by gases and small particles that did not undergo dry deposition or wet scavenging during transport, as well as by new particles formed in situ from the remaining emissions. As a consequence, new CCN may arise from nucleation and subsequent growth processes.

A closer look at the PNC maps for particles in the accumulation mode (ac0 in Figures 13a–13d) reveals that, although larger contributions of fire emissions to $PM_{2.5}$ took place some distance away from (to the northwest and north of) the SPMA, their impacts on the PNC of aerosol particles in the accumulation mode were found to occur primarily over the SPMA, where concentrations, on the order of 900 and 2,300 cm^{-3} (approximately 8% and 20% of the baseline-weighted relative differences), were detected (see Figures 13a and 13c). Larger differences in predicted PNC for particles in the accumulation mode over the SPMA are in agreement with larger differences in predicted particle mass concentrations for this size range and are

related to in situ secondary formation processes involving pollutants originating from biomass burning as well as those emitted locally. Similar calculations to those showed in Figure 12 but for other aerosol species, mainly NO_3, reveals that fire emissions contributed to secondary aerosol formation within the same region as they did for PNC. The nighttime chemistry of NO_3, initiated by the relatively slow oxidation of NO_2 by O_3, is the primary process by which certain unsaturated hydrocarbons lower their vapor pressure and are hence converted to low-volatility compounds (Kroll & Seinfeld, 2008; Monks, 2005). Once low-volatility compounds are produced, preexisting particles in the Aitken size range may then grow larger by condensation of those compounds onto their surfaces or by coagulation, giving rise to new particles in the accumulation mode. Aerosol particles arriving at SPMA from fire regions are exposed to such aging processes, thus changing their size distribution properties while being transported. In polluted urban environments, NO_3 can also serve as a source of organic nitrates and ammonium nitrate (Backman et al., 2012; Hallquist et al., 2009), thereby contributing to additional secondary aerosol mass. Fire impacts on the concentration of organic nitrates, which are lumped into one WRF-Chem species, were observed over the SPMA, although in small concentrations less than 1 ppb.

In terms of predicted OC, EC, and SOA contributions to the total PM_1 mass at the IAGU site, the mass percentages increased roughly in proportion to the increase of FINN particulate and ozone precursor emissions from 49.1%, 9.3%, and 12%, respectively, for BBE to 49.6%, 9.5%, and 12.6%, respectively, for 3BBE.

Predicted aerosol extinction profiles derived from the BBE and 3BBE simulations differ slightly near the surface but are blended at higher altitudes (see Figure 9). The observed and predicted profiles both show that aerosols were mostly confined to below 4 km in altitude. Most of the aerosols measured on 26 August were trapped and well mixed within the PBL, which reached a maximum altitude of 750 m; however, the lidar system detected two additional aerosol layers above the PBL: one at 1,200–2,000 m and one at 2,600–4,000 m. Similarly, most of the aerosol loadings measured on 1 September were concentrated within the PBL (maximum altitude of 1,100 m) with a second aerosol layer above it, at 2,400–3,800 m. When aerosol layers are detected above the PBL during the burning season (from August to October), they may be associated with the long-range transport of particles originating mainly from biomass burning events in the central west region of Brazil (Lopes et al., 2014; Miranda et al., 2017). Larger impacts of fire emissions on AOD during the fire emission contribution period were identified not only in the same region as they did for $PM_{2.5}$ but also over the southwestern part (coastal side) of the SPMA, which was quite likely due to an increase in the water uptake by aerosols as well as to a redistribution of aerosols at higher altitudes (see Figure 13i and 13k).

4.4. CCN

Although an appropriate evaluation of CCN activation in terms of chemical composition was not possible to perform due to a lack of concurrent size-resolved PM composition measurements, depending on the magnitude of the fire events and wind direction, the differences in the predicted CCN (BBE-BASE and 3BBE-BASE for CCN, as shown in Figures 10 and 13) suggest that OC (and hence SOAs) is one of the major contributors, if not the major contributor, to CCN activation in the SPMA. Previous field studies conducted around the world have shown that biomass burning events can influence the total PNC and CCN concentrations (Mallet et al., 2017), major impacts being attributable to the increased organic mass (Bougiatioti et al., 2016). Aging processes by coagulation of particles can alter the particle hygroscopicity, converting small hydrophobic particles into larger and hydrophilic ones, thus increasing the CCN activation of aerosols. Likewise, large hydrophilic particles may lower their hygroscopicity by incorporating small hydrophobic particles, leading to less activated particles. The overall impact of these interactions in WRF-Chem is primarily accounted for by the chemical composition, through the volume-weighted average hygroscopicity of each aerosol component, as coating effects are not treated in the model. In the present study, the maximum differences in the predicted CCN and PNC correlated well with each other (see Figures 13a and 13e and Figures 13c and 13g). In terms of spatial distribution, the larger contributions of fire emissions during the fire emission contribution period were in the same regions as those identified for PNC (see Figures 13a–13d and 13e–13h) and were related to the formation of highly hygroscopic aerosols, mainly NO_3. Over the SPMA, fire emissions contributed approximately 8% (600 cm^{-3}) and 20% (1,400 cm^{-3}) of the baseline CCN-weighted relative differences, respectively, for BBE and 3BBE (see Figures 13f and 13h). Slight increases in CCN during the second half of the period likely arose from aging processes among the surviving particles, as precipitation events occurred throughout the SPMA during that time.

5. Summary and Conclusions

The WRF-Chem community model was applied to investigate the impact of fire emissions on aerosol loadings and properties over the SPMA. To that end, we ran three sets of 18-day nested simulations, one without fire emissions (baseline simulations) and two including fire emissions with scaling factors of 1 and 3 for particulate and ozone precursor emissions (sensitivity simulations), covering the period from 17 August to 3 September 2014. Model results were evaluated against the available ground-, satellite-, and lidar-based measurements from the 2014 NUANCE-SPS campaign. Overall, the comparisons showed that the model qualitatively captures most of the observed variations and trends in meteorological variables, as well as the observed concentrations of chemical species throughout the study period, those derived from the higher resolution model simulation with fire emissions (BBE and 3BBE) having been found to perform slightly better than those derived from the higher resolution model simulation without fire emissions (BASE). However, although predicted PM species and O_3 were found to agree well with the observations in terms of temporal variations and trends ($R > 0.6$ in most cases), the maximum concentrations were often underestimated, probably due to uncertainties in the emissions inventories as well as to inaccurate predictions of meteorological parameters. Although the meteorological conditions during the study period were not generally favorable for long-range transport into the SPMA, a 5-day transport event from 22 to 26 August, referred to throughout the text as the fire emission contribution period, was studied in detail in order to investigate further the influence of biomass burning on aerosol properties over this area. This transport event would have brought elevated gas and aerosol concentrations from fire regions when the favorable meteorological conditions and fire events coincided. However, according to model results, biomass burning, on average, accounted for 8–24% (5–15 $\mu g/m^3$) and for 15–32% (12–26 $\mu g/m^3$) of maximum $PM_{2.5}$ and O_3 concentrations, respectively, suggesting that air pollutant levels depend largely on local emissions. The model also revealed that the largest fire impacts on $PM_{2.5}$, with relative differences of 27–72% (10–35 $\mu g/m^3$), took place northwest and north of the SPMA, within the inland portion of the state. In contrast, we found that the largest impacts on PNC did not take place within the same area as they did for $PM_{2.5}$; rather, maximum concentration differences were detected over the SPMA. As a consequence, new CCN arose in the same area. Biomass burning accounted for approximately 8–20% of the PNC- and CCN-weighted relative differences over the SPMA: 900–2,300 and 600–1,400 cm^{-3}, respectively. Despite the fact that small signs of fire emissions were seen over the SPMA (mostly weak fire events occurring during the fire emission contribution period), we can conclude that the impacts of air pollutants resulting from fire events are dependent on the magnitude of those events, not only for $PM_{2.5}$ and O_3 but also for the formation of CCN.

Acknowledgments

Angel Vara-Vela, Maria de Fatima Andrade, Yang Zhang, and Prashant Kumar thank the University Global Partnership Network (UGPN) for the collaborative funding received for the projects entitled *Towards the Treatment of Aerosol Emissions from Biomass Burning in Chemical Transport Models through a case study in the Metropolitan Area of São Paulo (BIOBURN)* and *Next-Generation Environmental Sensing for Local To Global Scale Health Impact Assessment (NEST-SEAS)*. Angel Vara-Vela and Maria de Fatima Andrade acknowledge the funding received from the Brazilian *Conselho Nacional de Desenvolvimento Científico e Tecnológico* (CNPq, National Council for Scientific and Technological Development), the Brazilian *Coordenação de Aperfeiçoamento de Pessoal de Nível Superior* (CAPES, Office for the Advancement of Higher Education), and the *Fundação de Amparo à Pesquisa do Estado de São Paulo* (FAPESP, São Paulo Research Foundation; Grant 2008/58104-8), which made the experimental campaigns possible. Yang Zhang acknowledges the support received from the U.S. National Science Foundation Earth System Models (EaSM) program (Grant AGS-1049200) at North Carolina State University (NCSU). Fabio Lopes acknowledges the support received from FAPESP (Grant 2011/14365-5). We are also grateful to Khairunnisa Yahya and Kai Wang, of NCSU, as well as to Aura Lupascu, of the Institute for Advanced Sustainability Studies (IASS), for their helpful discussions on model inputs and setup and to Mario Gavidia-Calderon, of IAG-USP, for his help with some of the plots. Data sets and tools used for data analysis were obtained, free of charge after a simple registration process, from the National Center for Atmospheric Research (NCAR) Research Data Archive Computational & Information System Laboratory, the NCAR Atmospheric Chemistry Observations & Modeling Laboratory, the São Paulo State *Companhia de Tecnologia de Saneamento Ambiental* (CETESB, Environmental Protection Agency), and the NCAR Command Language software. The WRF-Chem model code modifications and local emissions preprocessor used to generate the results presented in this paper are available at https://doi.org/10.17632/txt3rjj9dk.2. Aerosol data from the 2014 NUANCE-SPS campaign are available at https://doi.org/10.17632/4dfbpkx9jc.1. The authors declare that they have no conflict of interest.

References

Abdul-Razzak, H., & Ghan, S. J. (2000). A parameterization of aerosol activation: 2. Multiple aerosol types. *Journal of Geophysical Research*, *105*, 6837–6844. https://doi.org/10.1029/1999JD901161

Ahmadov, R., McKeen, S. A., Robinson, A. L., Bahreini, R., Middlebrook, A. M., De Gouw, J. A., et al. (2012). A volatility basis set model for summertime secondary organic aerosols over the eastern United States in 2006. *Journal of Geophysical Research*, *117*, D06301. https://doi.org/10.1029/2011JD016831

Almeida, G. P., Brito, J., Morales, C. A., Andrade, M. F., & Artaxo, P. (2014). Measured and modelled cloud condensation nuclei (CCN) concentration in São Paulo, Brazil: The importance of aerosol size-resolved chemical composition on CCN concentration prediction. *Atmospheric Chemistry and Physics*, *14*(14), 7559–7572. https://doi.org/10.5194/acp-14-7559-2014

Alves, N. O., Brito, J., Caumo, S., Arana, A., Hacon, S. S., Artaxo, P., et al. (2015). Biomass burning in the Amazon region: Aerosol source apportionment and associated health risk assessment. *Atmospheric Environment*, *120*, 277–285. https://doi.org/10.1016/j.atmosenv.2015.08.059

Alves, N. O., Vessoni, A. T., Quinet, A., Fortunato, R. S., Kajitani, G. S., Peixoto, M. S., et al. (2017). Biomass burning in the Amazon region causes DNA damage and cell death in human lung cells. *Scientific Reports*, *7*(1), 10,937. https://doi.org/10.1038/s41598-017-11024-3

Andrade, M. F., Ynoue, R. Y., Freitas, E. D., Todesco, E., Vara-Vela, A., Ibarra, S., et al. (2015). Air quality forecasting system for southeastern Brazil. *Frontiers in Environmental Science*, *3*, 1–14.

Archer-Nicholls, S., Lowe, D., Darbyshire, E., Morgan, W. T., Bela, M. M., Pereira, G., et al. (2015). Characterising Brazilian biomass burning emissions using WRF-Chem with MOSAIC sectional aerosol. *Geoscientific Model Development*, *8*(3), 549–577. https://doi.org/10.5194/gmd-8-549-2015

Artaxo, P., Rizzo, L. V., Brito, J. F., Barbosa, H. M. J., Arana, A., Sena, E. T., et al. (2013). Atmospheric aerosols in Amazonia and land use change: From natural biogenic to biomass burning conditions. *Faraday Discussions*, *165*, 203–235. https://doi.org/10.1039/c3fd00052d

Backman, J., Rizzo, L. V., Hakala, J., Nieminen, T., Manninen, H. E., Morais, F., et al. (2012). On the diurnal cycle of urban aerosols, black carbon and the occurrence of new particle formation events in springtime São Paulo, Brazil. *Atmospheric Chemistry and Physics*, *12*(23), 11,733–117,51. https://doi.org/10.5194/acp-12-11733-2012

Barth, M., Pfister, G., Wiedinmyer, C., Emmons, L., & Kumar, R. (2015). Biogenic, fire, lightning emissions and chemical boundary conditions, atmospheric chemistry observations & modeling, Boulder, Colo.

Bevan, S. L., North, P. R. J., Grey, W. M. F., Los, S. O., & Plummer, S. E. (2009). Impact of atmospheric aerosol from biomass burning on Amazon dry-season drought. *Journal of Geophysical Research*, *114*, D09204. https://doi.org/10.1029/2008JD011112

Binkowski, F. S., & Shankar, U. (1995). The regional particulate model, 1. Model description and preliminary results. *Journal of Geophysical Research*, *100*, 26,191–26,209. https://doi.org/10.1029/95JD02093

Birch, M. E., & Cary, R. A. (1996). Elemental carbon-based method for occupational monitoring of particulate diesel exhaust: Methodology and exposure issues. *Aerosol Science and Technology*, *25*(3), 221–241. https://doi.org/10.1080/02786829608965393

Boucher, O., Randall, D., Artaxo, P., Bretherton, C., Feingold, G., Forster, P., et al. (2013). Clouds and aerosols. In T. F. Stocker, D. Qin, G.-K. Plattner, M. Tignor, S. K. Allen, et al. (Eds.), *Climate change 2013: The physical science basis. Contribution of Working Group I to the Fifth Assessment Report of the Intergovernmental Panel on Climate Change*, (pp. 571–657). Cambridge, United Kingdom and New York, NY, USA: Cambridge University Press.

Bougiatioti, A., Bezantakos, S., Stavroulas, I., Kalivitis, N., Kokkalis, P., Biskos, G., et al. (2016). Biomass-burning impact on CCN number, hygroscopicity and cloud formation during summertime in the eastern Mediterranean. *Atmospheric Chemistry and Physics*, *16*(11), 7389–7409. https://doi.org/10.5194/acp-16-7389-2016

Boylan, J. W., & Russell, A. G. (2006). PM and light extinction model performance metrics, goals, and criteria for three-dimensional air quality models. *Atmospheric Environment*, *40*(26), 4946–4959. https://doi.org/10.1016/j.atmosenv.2005.09.087

Cai, C.-J., Zhang, X., Wang, K., Zhang, Y., Wang, L.-T., Zhang, Q., et al. (2016). Incorporation of new particle formation and early growth treatments into WRF/Chem: Model improvement, evaluation, and impacts of anthropogenic aerosols over East Asia. *Atmospheric Environment Part B*, *124*, 262–284. https://doi.org/10.1016/j.atmosenv.2015.05.046

Chapman, E. G., Gustafson, W. L. Jr., Easter, R. C., Barnard, J. C., Ghan, S. J., Pekour, M. S., & Fast, J. D. (2009). Coupling aerosol-cloud-radiative processes in the WRF-Chem model: Investigating the radiative impact of elevated point sources. *Atmospheric Chemistry and Physics*, *9*(3), 945–964. https://doi.org/10.5194/acp-9-945-2009

Che, H. C., Zhang, X. Y., Zhang, L., Wang, Y. Q., Zhang, Y. M., Shen, X. J., et al. (2017). Prediction of size-resolved number concentration of cloud condensation nuclei and long-term measurements of their activation characteristics. *Scientific Reports*, *7*(1), 5819. https://doi.org/10.1038/s41598-017-05998-3

Chen, F., & Dudhia, J. (2001). Coupling an advanced land surface-hydrology model with the Penn State-NCAR MM5 modeling system, Part I: Model implementation and sensitivity. *Monthly Weather Review*, *129*(4), 569–585. https://doi.org/10.1175/1520-0493(2001)129<0569:CAALSH>2.0.CO;2

Chen, S., Zhao, C., Qian, Y., Leung, L. R., Huang, J., Huang, Z., et al. (2014). Regional modeling of dust mass balance and radiative forcing over East Asia using WRF-Chem. *Aeolian Research*, *15*, 15–30. https://doi.org/10.1016/j.aeolia.2014.02.001

Easter, R. C., Ghan, S. J., Zhang, Y., Saylor, R. D., Chapman, E. G., Laulainen, N. S., et al. (2004). MIRAGE: Model description and evaluation of aerosols and trace gases. *Journal of Geophysical Research*, *109*, D20210. https://doi.org/10.1029/2004JD004571

Emmons, L. K., Walters, S., Hess, P. G., Lamarque, F., Pfister, G. G., Fillmore, D., et al. (2010). Description and evaluation of the Model for Ozone and Related chemical Tracers, version 4 (MOZART-4). *Geoscientific Model Development*, *3*(1), 43–67. https://doi.org/10.5194/gmd-3-43-2010

Environmental Protection Agency (2007). Guidance on the use of models and other analyses for demonstrating attainment of air quality goals for ozone, $PM_{2.5}$, and Regional Haze. U.S. Environmental Protection Agency, Research Triangle Park, NC.

Fast, J. D., Gustafson, W. I., Easter, R. C., Zaveri, R. A., Barnard, J. C., Chapman, E. G., et al. (2006). Evolution of ozone, particulates, and aerosol direct radiative forcing in the vicinity of Houston using a fully coupled meteorology-chemistry-aerosol module. *Journal of Geophysical Research*, *111*, D21305. https://doi.org/10.1029/2005JD006721

Forkel, R., Werhahn, J., Hansen, A. B., McKeen, S., Peckham, S., Grell, G., & Suppan, P. (2012). Effect of aerosol-radiation feedback on regional air quality—A case study with WRF/Chem. *Atmospheric Environment*, *53*, 202–211. https://doi.org/10.1016/j.atmosenv.2011.10.009

Freitas, S. R., Longo, K. M., Chatfield, R., Latham, D., Silva Dias, M. A. F., Andreae, M. O., et al. (2007). Including the sub-grid scale plume rise of vegetation fires in low resolution atmospheric transport models. *Atmospheric Chemistry and Physics*, *7*(13), 3385–3398. https://doi.org/10.5194/acp-7-3385-2007

Gelencser, A., Hoffer, A., Kiss, G., Tombacz, E., Kurdi, R., & Bencze, L. (2003). In-situ formation of light-absorbing organic matter in cloud water. *Journal of Atmospheric Chemistry*, *45*(1), 25–33. https://doi.org/10.1023/A:1024060428172

Gong, S., Barrie, L. A., & Blanchet, J. P. (1997). Modeling sea salt aerosols in the atmosphere: 1. Model development. *Journal of Geophysical Research*, *102*, 3805–3818. https://doi.org/10.1029/96JD02953

Grell, G. A., Freitas, S. R., Stuefer, M., & Fast, J. (2011). Inclusion of biomass burning in WRF-Chem: Impact of wildfires on weather forecasts. *Atmospheric Chemistry and Physics*, *11*(11), 5289–5303. https://doi.org/10.5194/acp-11-5289-2011

Grell, G. A., Peckham, S. E., Schmitz, R., McKeen, S. A., Wilczak, J., & Eder, B. (2005). Fully coupled "online" chemistry within the WRF model. *Atmospheric Environment*, *39*(37), 6957–6975. https://doi.org/10.1016/j.atmosenv.2005.04.027

Guenther, A., Karl, T., Harley, P., Wiedinmyer, C., Palmer, P. I., & Geron, C. (2006). Estimates of global terrestrial isoprene emissions using MEGAN (Model of Emissions of Gases and Aerosols from Nature). *Atmospheric Chemistry and Physics*, *6*(11), 3181–3210. https://doi.org/10.5194/acp-6-3181-2006

Gustafson, W. I. Jr., Chapman, E. G., Ghan, S. J., & Easter, R. C. (2007). Impact on modelled cloud characteristics due to simplified treatment of uniform cloud condensation nuclei during NEAQS 2004. *Geophysical Research Letters*, *34*, L19809. https://doi.org/10.1029/2007GL030021

Hallquist, M., Wenger, J. C., Baltensperger, U., Rudich, Y., Simpson, D., Claeys, M., et al. (2009). The formation, properties and impact of secondary organic aerosol: Current and emerging issues. *Atmospheric Chemistry and Physics*, *9*(14), 5155–5236. https://doi.org/10.5194/acp-9-5155-2009

Hartmann, D. L., Klein Tank, A. M. G., Rusticucci, M., Alexander, L. V., Bronnimann, S., et al. (2013). Observations: Atmosphere and surface. In T. F. Stocker, D. Qin, G. K. Plattner, M. Tignor, S. K. Allen, J. Boschung, et al. (Eds.), *Climate change 2013: The physical science basis. Contribution of Working Group I to the Fifth Assessment Report of the Intergovernmental Panel on Climate Change*. Cambridge, United Kingdom and New York, NY, USA: Cambridge University Press.

Hoelzemann, J. J., Longo, K. M., Fonseca, R. M., do Rosario, N. M. E., Elbern, H., Freitas, S. R., & Pires, C. (2009). Regional representativity of AERONET observation sites during the biomass burning season in South America determined by correlation studies with MODIS aerosol optical depth. *Journal of Geophysical Research*, *114*, D13301. https://doi.org/10.1029/2008JD010369

Hong, S. Y., Noh, Y., & Dudhia, J. (2006). A new vertical diffusion package with an explicit treatment of entrainment processes. *Monthly Weather Review*, *134*(9), 2318–2341. https://doi.org/10.1175/MWR3199.1

Hoshyaripour, G., Brasseur, G., Andrade, M. F., Gavidia-Calderon, M., Bouarar, I., & Ynoue, R. Y. (2016). Prediction of ground-level ozone concentration in São Paulo, Brazil: Deterministic versus statistic models. *Atmospheric Environment*, *145*, 365–375. https://doi.org/10.1016/j.atmosenv.2016.09.061

Iacono, M. J., Delamere, J. S., Mlawer, E. J., Shephard, M. W., Clough, S. A., & Collins, W. D. (2008). Radiative forcing by long-lived greenhouse gases: Calculations with the AER radiative transfer models. *Journal of Geophysical Research*, *113*, D13103. https://doi.org/10.1029/2008JD009944

Ichoku, C., Kahn, R., & Chin, M. (2012). Satellite contributions to the quantitative characterization of biomass burning for climate modeling, *Atmospheric Research*, *111*, 1–28, https://doi.org/10.1016/j.atmosres.2012.03.007

Janssens-Maenhout, G., Crippa, M., Guizzardi, D., Dentener, F., Munteau, M., Pouliot, G., et al. (2015). HTAP_v2.2: A mosaic of regional and global emission grid maps for 2008 and 2010 to study hemispheric transport of air pollution. *Atmospheric Chemistry and Physics*, *15*(19), 11,411–11,432. https://doi.org/10.5194/acp-15-11411-2015

Jiménez, P. A., Dudhia, J., González-Rouco, J. F., Navarro, J., Montávez, J. P., & García-Bustamante, E. (2012). A revised scheme for the WRF surface layer formulation. *Monthly Weather Review*, *140*(3), 898–918. https://doi.org/10.1175/MWR-D-11-00056.1

Jones, S., & Creighton, G. (2011). AFWA dust emission scheme for WRF/Chem-GOCART, In: 2011 WRF Workshop, June 20–24, Boulder, CO, USA.

Kong, X., Forkel, R., Sokhi, R. S., Suppan, P., Baklanov, A., Gauss, M., et al. (2015). Analysis of meteorology-chemistry interactions during air pollution episodes using online coupled models within AQMEII phase-2. *Atmospheric Environment*, *115*, 527–540. https://doi.org/10.1016/j.atmosenv.2014.09.020

Kroll, J. H., & Seinfeld, J. H. (2008). Chemistry of secondary organic aerosol: Formation and evolution of low-volatility organics in the atmosphere. *Atmospheric Environment*, *42*(16), 3593–3624. https://doi.org/10.1016/j.atmosenv.2008.01.003

Kulmala, M., Laaksonen, A., & Pirjola, L. (1998). Parameterizations for sulfuric acid/water nucleation rates. *Journal of Geophysical Research*, *103*, 8301–8307. https://doi.org/10.1029/97JD03718

Kusaka, H., Kondo, H., Kikegawa, Y., & Kimura, F. (2001). A simple single-layer urban canopy model for atmospheric models: Comparison with multi-layer and slab models. *Boundary-Layer Meteorology*, *101*(3), 329–358. https://doi.org/10.1023/A:1019207923078

Lance, S., Medina, J., Smith, J. N., & Nenes, A. (2006). Mapping the operation of the DMT continuous flow CCN counter. *Aerosol Science and Technology*, *40*(4), 242–254. https://doi.org/10.1080/02786820500543290

Lopes, F. J. S., Moreira, G. A., Rodrigues, P. F., Guerrero-Rascado, J. L., Andrade, M. F., & Landulfo, E. (2014). Lidar measurements of tropospheric aerosol and water vapor profiles during the winter season campaigns over the metropolitan area of São Paulo, Brazil, Proceedings of SPIE, Lidar Technologies, Techniques, and Measurements for Atmospheric Remote Sensing X, 92460H, https://doi.org/10.1117/12.2067374.

Mallet, M. D., Cravigan, L. T., Milic, A., Alroe, J., Ristovski, Z. D., Ward, J., et al. (2017). Composition, size and cloud condensation nuclei activity of biomass burning aerosol from northern Australian savannah fires. *Atmospheric Chemistry and Physics*, *17*(5), 3605–3617. https://doi.org/10.5194/acp-17-3605-2017

Marple, V. A., Rubow, K. L., Ananth, G. P., & Fissan, H. J. (1986). Micro-orifice uniform deposit impactor. *Journal of Aerosol Science*, *17*(3), 489–494. https://doi.org/10.1016/0021-8502(86)90141-2

Mass, C., & Ovens, D. (2010). WRF model physics: Progress, problems, and perhaps some solutions, the 11th WRF User's workshop, Boulder, Colo., 21–25 June.

Merikanto, J., Spracklen, D. V., Mann, G. W., Pickering, S. J., & Carslaw, K. S. (2009). Impact of nucleation on global CCN. *Atmospheric Chemistry and Physics*, *9*(21), 8601–8616. https://doi.org/10.5194/acp-9-8601-2009

Mie, G. (1908). Beiträge zur Optik trüber Medien, speziell kolloidaler Metallösungen. *Annals of Physics*, *330*(3), 377–445. https://doi.org/10.1002/andp.19083300302

Miranda, R. M., Lopes, F., Rosario, N. E., Yamasoe, M. A., Landulfo, E., & Andrade, M. F. (2017). The relationship between aerosol particles chemical composition and optical properties to identify the biomass burning contribution to fine particles concentration: A case study for São Paulo city, Brazil. *Environmental Monitoring and Assessment*, *189*, 9–15.

Molod, A., Takacs, L. L., Suarez, M. J., Bacmeister, J. T., Song, I. S., & Eichmann, A. (2012). The GEOS-5 atmospheric general circulation model: Mean climate and development from MERRA to fortuna. NASA Technical Memorandum 104606, Vol. 28, Technical Report Series on Global Modeling and Data Assimilation, edited by: Suarez, M. J., 117 pp.

Monks, P. S. (2005). Gas-phase radical chemistry in the troposphere. *Chemical Society Reviews*, *34*(5), 376–395. https://doi.org/10.1039/b307982c

Moreira, D. S., Longo, K. M., Freitas, S. R., Yamasoe, M. A., Mercado, L. M., Rosário, N. E., et al. (2017). Modeling the radiative effects of biomass burning aerosols on carbon fluxes in the Amazon region. *Atmospheric Chemistry and Physics*, *17*(23), 14,785–14,810. https://doi.org/10.5194/acp-17-14785-2017

Morrison, H., Thompson, G., & Tatarskii, V. (2009). Impact of cloud microphysics on the development of trailing stratiform precipitation in a simulated squall line: Comparison of one- and two-moment schemes. *Monthly Weather Review*, *137*(3), 991–1007. https://doi.org/10.1175/2008MWR2556.1

Oyama, B. S., Andrade, M. F., Herckes, P., Dusek, U., Rockmann, T., & Holzinger, R. (2016). Chemical characterization of organic particulate matter from on-road traffic in São Paulo, Brazil. *Atmospheric Chemistry and Physics*, *16*(22), 14,397–14,408. https://doi.org/10.5194/acp-16-14397-2016

Pankow, J. F. (1994a). An absorption model of the gas aerosol partitioning involved in the formation of secondary organic aerosol. *Atmospheric Environment*, *28*(2), 185–188. https://doi.org/10.1016/1352-2310(94)90093-0

Pankow, J. F. (1994b). An absorption model of the gas aerosol partitioning involved in the formation of secondary organic aerosol. *Atmospheric Environment*, *28*(2), 189–193. https://doi.org/10.1016/1352-2310(94)90094-9

Pereira, G., Siqueira, R., Rosario, N. E., Longo, K. L., Freitas, S. R., Cardozo, F. S., et al. (2016). Assessment of fire emission inventories during the South American Biomass Burning Analysis (SAMBBA) experiment. *Atmospheric Chemistry and Physics*, *16*(11), 6961–6975. https://doi.org/10.5194/acp-16-6961-2016

Pereira, G. M., Teinila, K., Custódio, D., Santos, A. G., Xian, H., Hillamo, R., et al. (2017). Particulate pollutants in the Brazilian city of São Paulo: 1-year investigation for the chemical composition and source apportionment. *Atmospheric Chemistry and Physics*, *17*(19), 11,943–11,969. https://doi.org/10.5194/acp-17-11943-2017

Roberts, G. C., & Nenes, A. (2005). A continuous-flow streamwise thermal-gradient CCN chamber for atmospheric measurements. *Aerosol Science and Technology*, *39*(3), 206–221. https://doi.org/10.1080/027868290913988

Rozante, J. R., Moreira, D. S., Gonçalves, L. G. G., & Vila, D. A. (2010). Combining TRMM and surface observations of precipitation: Technique and validation over South America. *Weather and Forecasting*, *25*(3), 885–894. https://doi.org/10.1175/2010WAF2222325.1

Sarwar, G., Fahey, K., Napelenok, S., Roselle, S., & Mathur, R. (2011). Examining the impact of CMAQ model updates on aerosol sulfate predictions, the 10th annual CMAS Models-3 User's conference, October, Chapel Hill, N. C.

Sarwar, G., Luecken, D., & Yarwood, G. (2007). Chapter 2.9 developing and implementing an updated chlorine chemistry into the community multiscale air quality model. *Developments in Environmental Science*, *6*, 168–176. https://doi.org/10.1016/S1474-8177(07)06029-9

Scott, C. E., Rap, A., Spracklen, D. V., Forster, P. M., Carslaw, K. S., Mann, G. W., et al. (2014). The direct and indirect radiative effects of biogenic secondary organic aerosol. *Atmospheric Chemistry and Physics*, *14*(1), 447–470. https://doi.org/10.5194/acp-14-447-2014

Seinfeld, J. H., Bretherton, C., Carslaw, K. S., Coe, H., DeMott, P. J., Dunlea, E. J., et al. (2016). Improving our fundamental understanding of the role of aerosol–cloud interactions in the climate system. *PNAS*, *113*(21), 5781–5790. https://doi.org/10.1073/pnas.1514043113

Skamarock, W. C., Klemp, J. B., Dudhia, J., Gill, D. O., Barker, D. M., Wang, W., & Powers, J. G. (2008). A description of the advanced research WRF version 3, NCAR tech. Note, NCAR/TN-475+STR, Natl. Cent. Atmos. Res., Boulder, Colo.

Souto-Oliveira, C. E., Andrade, M. F., Kumar, P., Lopes, F. J. D., Babinski, M., & Landulfo, E. (2016). Effect of vehicular traffic, remote sources and new particle formation on the activation properties of cloud condensation nuclei in the megacity of São Paulo, Brazil. *Atmospheric Chemistry and Physics*, *16*(22), 14,635–14,656. https://doi.org/10.5194/acp-16-14635-2016

Spracklen, D. V., Carslaw, K. S., Kulmala, M., Kerminen, V. M., Mann, G. W., & Sihto, S. L. (2006). The contribution of boundary layer nucleation events to total particle concentrations on regional and global scales. *Atmospheric Chemistry and Physics*, *6*(12), 5631–5648. https://doi.org/10.5194/acp-6-5631-2006

Takemura, T., Nakajima, T., Dubovik, O., Holben, B. N., & Kinne, S. (2002). Single-scattering albedo and radiative forcing of various aerosol species with a global three-dimensional model. *Journal of Climate*, *15*(4), 333–352. https://doi.org/10.1175/1520-0442(2002)015<0333:SSAARF>2.0.CO;2

Tie, X., Madronich, S., Walters, S., Zhang, R., Racsh, P., & Collins, W. (2003). Effect of clouds on photolysis and oxidants in the troposphere. *Journal of Geophysical Research*, *108*(D20), 4642. https://doi.org/10.1029/2003JD003659

Tuccella, P., Curci, G., Grell, G. A., Visconti, G., Crumeyrolle, S., Schwarzenboeck, A., & Mensah, A. A. (2015). A new chemistry option in WRF-Chem v 3.4 for the simulation of direct and indirect aerosol effects using VBS: Evaluation against IMPACT-EUCAARI data. *Geoscientific Model Development*, *8*(9), 2749–2776. https://doi.org/10.5194/gmd-8-2749-2015

Tuccella, P., Curci, G., Visconti, G., Bessagnet, B., Menut, L., & Park, R. J. (2012). Modeling of gas and aerosol with WRF/Chem over Europe: Evaluation and sensitivity study. *Journal of Geophysical Research*, *117*, D03303. https://doi.org/10.1029/2011JD016302

Vara-Vela, A., Andrade, M. F., Kumar, P., Ynoue, R. Y., & Muñoz, A. G. (2016). Impact of vehicular emissions on the formation of fine particles in the Sao Paulo metropolitan area: A numerical study with the WRF-Chem model. *Atmospheric Chemistry and Physics*, *16*(2), 777–797. https://doi.org/10.5194/acp-16-777-2016

Vara-Vela, A., Muñoz, A. G., Lomas, A., González, C. M., Gavidia-Calderon, M., & Andrade, M. F. (2017). The another Assimilation System for WRF-Chem (AAS4WRF): A new mass-conserving emissions preprocessor for WRF-Chem regional modelling, Abstract A53F-2343, 2017 AGU Fall Meeting, New Orleans, LA.

Wang, K., Zhang, Y., Yahya, K., Wu, S.-Y., & Grell, G. (2015). Implementation and initial application of new chemistry-aerosol options in WRF/Chem for simulating secondary organic aerosols and aerosol indirect effects for regional air quality, *Atmospheric Environment*, *115*, 716–732. https://doi.org/10.1016/j.atmosenv.2014.12.007

Whitby, E. R., McMurry, P. H., Shankar, U., & Binkowski, F. S. (1991). Modal aerosol dynamics (Pembroke, Ont.) modeling, Rep. 600/3–91/020, Atmospheric Research and Exposure Assessment The Laboratory, US Environmental Protection Agency, Research Triangle Park, NC, 1991.

Wiedinmyer, C., Akagi, S. K., Yokelson, R. J., Emmons, L. K., Al-Saadi, J. A., Orlando, J. J., & Soja, A. J. (2011). The Fire INventory from NCAR (FINN): A high resolution global model to estimate the emissions from open burning. *Geoscientific Model Development*, *4*(3), 625–641. https://doi.org/10.5194/gmd-4-625-2011

Winklmayr, W., Reischl, G. P., Lindner, A. O., & Berner, A. (1991). A new electromobility spectrometer for the measurement of aerosol size distributions in the size range from 1 to 1000 nm. *Journal of Aerosol Science*, *22*(3), 289–296. https://doi.org/10.1016/S0021-8502(05)80007-2

Yahya, K., He, J., & Zhang, Y. (2015). Multiyear applications of WRF/Chem over continental U. S.: Model evaluation, variation trend, and impacts of boundary conditions. *Journal of Geophysical Research: Atmospheres*, *20*, 12,748–12,777. https://doi.org/10.1002/2015JD023819

Yahya, K., Wang, K., Campbell, P., Chen, Y., Glotfelty, T., He, J., et al. (2017). Decadal application of WRF/Chem for regional air quality and climate modelling over the U. S. under the representative concentration pathways scenarios. Part 1: Model evaluation and impact of downscaling. *Atmospheric Environment*, *152*, 562–583. https://doi.org/10.1016/j.atmosenv.2016.12.029

Yahya, K., Wang, K., Zhang, Y., & Kleindienst, T. E. (2015). Application of WRF/Chem over North America under the AQMEII phase 2—Part 2: Evaluation of 2010 simulation and responses of air quality and meteorology-chemistry interactions to changes in emissions and meteorology from 2006 to 2010. *Geoscientific Model Development*, *8*(7), 2095–2117. https://doi.org/10.5194/gmd-8-2095-2015

Yarwood, G., Rao, S., Yocke, M., & Whitten, G. Z. (2005). Final report—Updates to the carbon bond chemical mechanism: CB05, Rep. RT-04-00675, 246 pp., Yocke and Co., Novato, Calif.

Zhang, Y. (2008). Online-coupled meteorology and chemistry models: History, current status, and outlook. *Atmospheric Chemistry and Physics*, *8*(11), 2895–2932. https://doi.org/10.5194/acp-8-2895-2008

Zhang, Y., Liu, P., Pun, B., & Seigneur, C. (2006). A comprehensive performance evolution of MM5-CMAQ for the summer 1999 southern oxidants study episode—Part I: Evaluation protocols, databases, and meteorological predictions. *Atmospheric Environment*, *40*(26), 4825–4838. https://doi.org/10.1016/j.atmosenv.2005.12.043

Zhang, Y., Wen, X.-Y., & Jang, C. J. (2010). Simulating chemistry-aerosol-cloud-radiation-climate feedbacks over the continental US using the online-coupled Weather Research Forecasting Model with chemistry (WRF/Chem). *Atmospheric Environment*, *44*(29), 3568–3582. https://doi.org/10.1016/j.atmosenv.2010.05.056

Zheng, Y., Alapaty, K. A., Herwehe, J. A., Del Genio, A. D., & Niyogi, D. (2016). Improving high resolution weather forecasts using the Weather Research and Forecasting (WRF) Model with an updated Kain-Fritsch scheme. *Monthly Weather Review*, *144*(3), 833–860. https://doi.org/10.1175/mwr-d-15-0005.1